Euro. Jnl of Applied Mathematics (2020), *vol.* 31, *pp.* 111–142
doi:10.1017/S0956792518000499

On the avascular ellipsoidal tumour growth model within a nutritive environment

GEORGE FRAGOYIANNIS[1], FOTEINI KARIOTOU[2] and PANAYIOTIS VAFEAS[1]

[1]*Department of Chemical Engineering, University of Patras, Patras, Greece*
email: vafeas@chemeng.upatras.gr; gfrago@chemeng.upatras.gr
[2]*School of Science and Technology, Hellenic Open University, Patras, Greece*
email: kariotou@eap.gr

(*Received 6 October 2017; revised 30 June 2018; accepted 21 July 2018; first published online 18 September 2018*)

The present work is part of a series of studies conducted by the authors on analytical models of avascular tumour growth that exhibit both geometrical anisotropy and physical inhomogeneity. In particular, we consider a tumour structure formed in distinct ellipsoidal regions occupied by cell populations at a certain stage of their biological cycle. The cancer cells receive nutrient by diffusion from an inhomogeneous supply and they are subject to also an inhomogeneous pressure field imposed by the tumour microenvironment. It is proved that the lack of symmetry is strongly connected to a special condition that should hold between the data imposed by the tumour's surrounding medium, in order for the ellipsoidal growth to be realizable, a feature already present in other non-symmetrical yet more degenerate models. The nutrient and the inhibitor concentration, as well as the pressure field, are provided in analytical fashion via closed-form series solutions in terms of ellipsoidal eigenfunctions, while their behaviour is demonstrated by indicative plots. The evolution equation of all the tumour's ellipsoidal interfaces is postulated in ellipsoidal terms and a numerical implementation is provided in view of its solution. From the mathematical point of view, the ellipsoidal system is the most general coordinate system that the Laplace operator, which dominates the mathematical models of avascular growth, enjoys spectral decomposition. Therefore, we consider the ellipsoidal model presented in this work, as the most general analytic model describing the avascular growth in inhomogeneous environment. Additionally, due to the intrinsic degrees of freedom inherited to the model by the ellipsoidal geometry, the ellipsoidal model presented can be adapted to a very populous class of avascular tumours, varying in figure and in orientation.

Key words: Mathematical modelling, boundary value problems, avascular tumour growth, ellipsoidal geometry

2010 Mathematics Subject Classification: 35J25, 35C10, 35K57, 92B99

1 Introduction

The prognosis of cancer tumour development has gainedmuch scientific interestover the last century due to its crucial importance on designing the best treatment option for the patient. The corresponding research refers to many different disciplines, since it concerns a very complicated phenomenon, including many interrelated procedures, which is still only partly understood.

The mathematical modelling of tumour growth offers much in the theoretical research in this field, since it saves time, funds and ethical confrontations. It aims to bring to light the dominant mechanisms and the most effective parameters of the phenomenon, keeping the need of *in vivo* experiments to the minimum. Nevertheless, a mathematical model cannot be but an approximation to the *in vivo* development of a tumour mass in a healthy tissue, so in order to have useful results one has to develop a mathematical model as close to reality as possible.

In this direction, a great deal of scientific effort has been made and the corresponding bibliography counts a massive mathematical model production within the last 50 years. Considering only a small subdivision of them, deterministic continuum models, amenable to analytic formulation and treatment, range in complexity with respect to the geometrical symmetry allowed in modelling the tumour's structure [2, 3, 5, 6, 16, 17, 21, 28, 30], to the degree of the cell heterogeneity or of the host medium's inhomogeneity [5, 6, 22, 28] or to the different scales taken into account, describing the corresponding processes that are involved in the model [2, 5, 11, 27–30].

Before we proceed, let us briefly outline the cancer tumour physiology. A tumour consists of cells that consume nutrients, proliferate many more times than normal cells do and die, either out of reaching the end of their cell cycle (in which case they are called apoptotic cells) or due to lack of nutrients or to external inhibitory agents (called then necrotic cells).

A cancer tumour starts to build up inside a healthy tissue after several concurrent incidents in cell physiology trigger tumorigenesis [12, 21, 25, 27]. The cancer colony receives nutrients from its surrounding medium by diffusion. As the colony becomes crowded, the nutrient level declines towards the tumour's centre, producing a corresponding decline of the cells vitality, which gradually leads to the formation of a necrotic core and to an observable delay on the tumour's growth [31]. With diffusion being the dominant mechanism for the nutrient supply and for the removal of the wastes, the tumour eventually reaches an equilibrium stage, where the cell volume gained by proliferation balances the cell volume loss due to necrosis and disintegration. The tumour size reaches a plateau which may be maintained for as long as the nutrient supply remains restricted. Such growth pause marks the end of the first phase of the tumour's evolution, called the avascular phase of tumour growth [2, 5, 21, 30]. As the time passes, the cancer colony may be either diminished, under effective surveillance from the immune system, or the next evolution phase may be activated by the onset of angiogenesis, characterised by the formation of new blood vessels that ensure unlimited nutrient supply. The invasive phase of vascular growth is then inevitable, leading to malignant and/or metastatic tumours [5, 12, 21, 25, 27, 31].

Much scientific effort has been devoted to studying the early phase of avascular growth, both because it is the step stone from which the invasive phase begins and also because it is a well-defined phase amenable to theoretical analysis and experimental reproducibility. Moreover, the mathematical modelling of the avascular growth allows carrying out thorough analytical studies of the phenomenon and for obtaining analytical results, thus providing clear insights on underlying mechanisms. In this work, the interest is focused on the avascular stage of tumour's evolution.

A feature characterising the avascular phase, apart that it ends with a phenomenological halt of the tumour's spatial evolution, is that during that phase, the tumour consists of distinct layers, each one occupied by cells at a certain phase of their cell cycle. In particular, as it was pointed out in the seminal work of Folkman and Hochberg [12] and used thereafter as basic geometrical structure in relative mathematical models, see, for example, [25] for an extensive review and references therein, a fully developed avascular tumour colony consists of an exterior rim, occupied by cells that are proliferating, and it is formed right next to the host tissue, receiving

https://doi.org/10.1017/S0956792518000499 Published online by Cambridge University Press

abundant nutrient. The subsequent layer is occupied by live but dormant cells, which envelopes the necrotic core, where all cells are either dead or disintegrated. As a consequence of nutrient diffusion and consumption, the different layers of the colony exhibit inwardly decreasing nutrient levels. The living cells' metabolic by-products as well as the by-products of the disintegration of necrotic cells inhibit proliferation and thus they are considered to be growth-inhibiting factors. Moreover, as a result of the growing cancerous mass, a layer occupied by normal cells is formed in the immediate vicinity of the tumour and it provides nutrient supply, while it also transmits the pressure, generated by the abnormal growth, from the host tissue to the tumour.

Most mathematical models of the avascular growth found in the literature concern radially symmetric layered structures growing in homogeneous suspensions, while small perturbations of the spherical configuration have also been considered [3, 5, 6, 11, 16, 17, 22, 28]. This is not surprising, since most avascular tumours cease their growth at such a size that small deviations from the spherical symmetry are considered quantitatively insignificant. However, there is evidence that mechanical effects influence both the size and the shape of the growing tumour [1, 7, 19, 32, 33]. In some previous works [9, 18, 22–24], the authors have investigated the effect of a non-symmetric tumour configuration on the prognosis of the tumour's evolution, by gradually relaxing the geometrical symmetry of the mathematical model from the one-dimensional spherical model to the two-dimensional (2D) axisymmetric oblate or prolate spheroidal one. It has been shown that certain qualitative features are revealed with the departure from radial symmetry, such as that there are special conditions needed to be fulfilled in order for non-symmetrical growth to be feasible. Moreover, it has been shown that in non-spherically symmetric models, the geometrical interfaces in the tumour structure do not coincide with the corresponding material ones, as it happens in the spherical case. However, small deviations from the initial spherical shape occur also in fully homogeneous environment, without imposing ad hoc boundary conditions or requiring any special conditions [4, 6, 22], while in [15] it is graphically shown that ellipsoidal and more complex shapes can appear from initially spherical tumours, even considering homogeneous and isotropic conditions.

In the present paper, we proceed this investigation with tackling the geometrically three dimensional (3D) anisotropic model of an avascular cancer colony, while maintaining the physical description of piecewise isotropic structure. In particular, we investigate the tumour's evolution, under the assumption that the colony exhibits an ellipsoidal configuration, attributed mostly to the pressure field imposed by the host tissue in the presence of inhomogeneous nutrient environment. Assuming an ellipsoidal model, the tumour's description in three dimensions inherits two degrees of freedom, namely the two eccentricities of the corresponding ellipsoidal system, in addition to its orientation. Thus, the model can be fairly adjusted quite accurately to most of the avascular tumours, considering their convexity and the regularity of their exterior boundary. Moreover, using ellipsoidal geometry we reach the limits of treating analytically the boundary value problems involved in the model. This is due to the fact that the dominant operator for such problems is the Laplace operator and the ellipsoidal system is the most general coordinate system with second-degree level surfaces, in which its spectral decomposition is tractable [8, 10, 20, 26].

Moreover, the tumour is considered to be lying in a bounded ellipsoidal inhomogeneous nutritive surrounding medium which, additionally to providing abundant nutrient supply, balances the pressure field resulting from the interaction of the growing cancerous mass and the surrounding tissue's restrictions. The pressure field is also considered inhomogeneous, and the exact conditions for the nutrient supply and for the pressure imposed, which ensure the

https://doi.org/10.1017/S0956792518000499 Published online by Cambridge University Press

ellipsoidal growth, are one of the scopes of the present work. Thus, in this paper we examine the most general analytic geometrical model of the avascular tumour growth supported by inhomogeneous data, where the physical parameters of the model, as the consumption or production rates, the diffusion constants and the cell motility parameters, are step functions with respect to the tumour compartments.

The article is organised as follows. In Section 2, the model is postulated as a system of three boundary value problems coupled with an ordinary differential equation in terms of ellipsoidal geometry. The underlying physical hypotheses of the model are also included here. Section 3 provides the solutions of the boundary value problems in an explicit analytical fashion, while the differential equation is expressed analytically in the form of a highly nonlinear equation, amenable to numerical elaboration. This task is accomplished in Section 5, where we additionally demonstrate the efficiency of the proposed model by implementing the obtained fields, while in Section 4 the reduction of the results obtained from the ellipsoidal model to more degenerate forms is included. A discussion section summarises the results of the present work, giving hints to further analysis and development of the model. Finally, an appendix with detailed information for obtaining the final analytical formulae completes the structure of this article.

2 Statement of the problem

We consider a unique confocal ellipsoidal coordinate system with foci $(0, \pm h_1, 0)$, $(\pm h_2, 0, 0)$, $(\pm h_3, 0, 0)$ [8] emanating from the reference ellipsoid, given in Cartesian coordinates as

$$\frac{x_1^2}{\alpha_1^2} + \frac{x_2^2}{\alpha_2^2} + \frac{x_3^2}{\alpha_3^2} = 1 \tag{2.1}$$

with $0 < \alpha_3 < \alpha_2 < \alpha_1 < +\infty$ and $h_1^2 = \alpha_2^2 - \alpha_3^2$, $h_2^2 = \alpha_1^2 - \alpha_3^2$ and $h_3^2 := h_2^2 - h_1^2 = \alpha_1^2 - \alpha_2^2$.

The ellipsoidal coordinates (ρ, ν, μ) of the point $\mathbf{r} \in \mathbb{R}^3$ are related to the corresponding Cartesian coordinates (x_1, x_2, x_3) via the relations

$$x_1^2 = \frac{\rho^2 \mu^2 \nu^2}{h_2^2 h_3^2} \tag{2.2}$$

$$x_2^2 = \frac{\left(\rho^2 - h_3^2\right)\left(\mu^2 - h_3^2\right)\left(h_3^2 - \nu^2\right)}{h_1^2 h_3^2} \tag{2.3}$$

and

$$x_3^2 = \frac{\left(\rho^2 - h_2^2\right)\left(h_2^2 - \mu^2\right)\left(h_2^2 - \nu^2\right)}{h_1^2 h_2^2}, \tag{2.4}$$

where the corresponding variables run within the intervals $\rho \geq h_2$, $\mu^2 \in \left[h_3^2, h_2^2\right]$ and $\nu^2 \in \left[0, h_3^2\right]$. We note that the Cartesian octants correspond to the ellipsoidal coordinates according to the following transformation rules [8]. The sign of x_1 is ruled by the sign of ν, the sign of x_2 is ruled by the corresponding sign of $\sqrt{h_3^2 - \nu^2}$ and the sign of x_3 is controlled in accordance to the sign of the ellipsoidal factor $\sqrt{h_2^2 - \mu^2}$. We also note that the reference ellipsoid inherits the confocal ellipsoidal system's semifocal distances h_1, h_2, h_3 and hereafter its semiaxes α_1, α_2, α_3 will no more appear in the model description.

https://doi.org/10.1017/S0956792518000499 Published online by Cambridge University Press

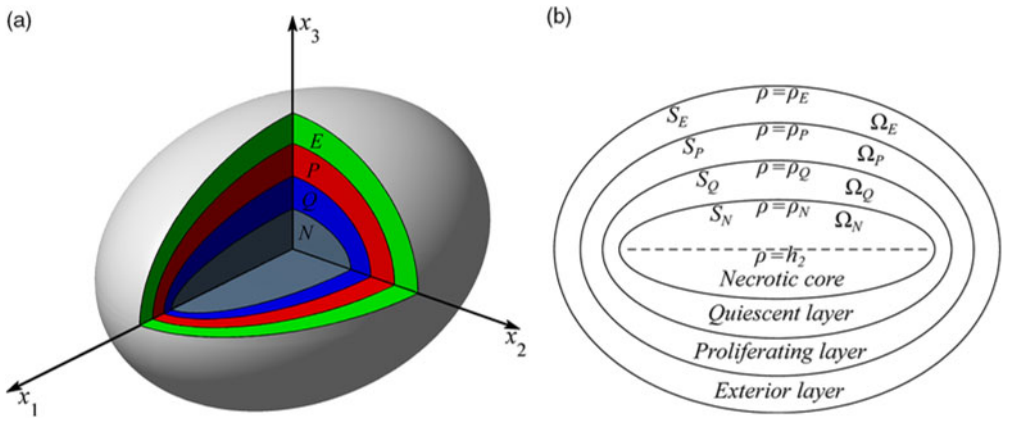

FIGURE 1. Three-shell avascular tumour growth model including (a) the 3D representation of the model's regions and (b) the detailed illustration of the corresponding spatial domains Ω_j and boundaries S_j on x_1x_3-plane with $j = N, Q, P, E$.

In terms of the ellipsoidal variables, the fully developed avascular tumour that we consider in our model is described as follows. We denote by Ω_j the ellipsoidal region in the tumour, occupied by cells at a certain stage of their biological cycle, characterized by constant density d_j, j indexing the different compartments as they will be designated in the next paragraph. The available nutrient concentration in $\mathbf{r} \in \Omega_j$ is denoted by $\sigma(\mathbf{r})$, while the concentration of the growth inhibiting agent is denoted by $\beta(\mathbf{r})$. Moreover, the tumour tissue is considered incompressible and compact; thus the cell gain or loss, due to proliferation and disintegration in each region, results in a pressure field $P(\mathbf{r})$. The gradient of the aforementioned parameters determines the cell movement with velocity $\mathbf{v}(\mathbf{r})$, so that a cell moves passively down the pressure gradient and towards regions rich in nutrient and poor in inhibitor concentration. The vital state of the cell occupying the geometrical point $\mathbf{r}$ depends on the nutrient concentration and on the inhibitor concentration available, with respect to the critical values $\sigma_N^*, \sigma_Q^*, \beta^*$ as follows. A cell is alive if and only if the nutrient level is above the critical concentration σ_N^*; it is in a mitotic dormant state if the nutrient varies in the interval $\left[\sigma_N^*, \sigma_Q^*\right)$ and proliferates when $\sigma(\mathbf{r}) \geq \sigma_Q^*$ and $\beta(\mathbf{r}) \leq \beta^*$.

In particular, the necrotic core, which is occupied by necrotic cells, is defined in ellipsoidal terms as $\Omega_N = \left\{(\rho, \mu, \nu) \in \mathbb{R}^3 : h_2 \leq \rho < \rho_N, h_3^2 \leq \mu^2 \leq h_2^2, 0 \leq \nu^2 \leq h_3^2\right\}$, while the next layer is occupied by quiescent cells and is defined as $\Omega_Q = \left\{(\rho, \mu, \nu) \in \mathbb{R}^3 : \rho_N \leq \rho < \rho_Q, h_3^2 \leq \mu^2 \leq h_2^2, 0 \leq \nu^2 \leq h_3^2\right\}$. The proliferating layer is comprised of $\Omega_P = \left\{(\rho, \mu, \nu) \in \mathbb{R}^3 : \rho_Q \leq \rho < \rho_P, h_3^2 \leq \mu^2 \leq h_2^2, 0 \leq \nu^2 \leq h_3^2\right\}$, while the whole cancer tumour is enveloped inside the healthy exterior layer defined via the domain $\Omega_E = \left\{(\rho, \mu, \nu) \in \mathbb{R}^3 : \rho_P \leq \rho < \rho_E, h_3^2 \leq \mu^2 \leq h_2^2, 0 \leq \nu^2 \leq h_3^2\right\}$, which is occupied by normal cells of the host tissue. The exterior ellipsoidal boundaries S_j of the above domains, correspond to the different values of the ellipsoidal variable $\rho = \rho_j$ with $j = N, Q, P, E$, respectively, and apparently it holds that $h_2 \leq \rho_N < \rho_Q < \rho_P < \rho_E$. The aforementioned modelling configuration is illustrated within Figure 1 for an intersection with the x_1x_3-plane.

On the exterior surface S_E, the surrounding medium provides nutrient in the form

$$\sigma_\infty(\mathbf{r}_E) = \sum_{l=0}^{\infty} \sum_{m=1}^{2l+1} \sigma_{\infty,l}^m(\rho_E) S_l^m(\mu,\nu) \text{ with } \mathbf{r}_E = (\rho_E,\mu,\nu) \in S_E) \tag{2.5}$$

https://doi.org/10.1017/S0956792518000499 Published online by Cambridge University Press

and imposes a pressure field

$$P_\infty(\mathbf{r}_E) = \sum_{l=0}^{\infty} \sum_{m=1}^{2l+1} p^m_{\infty,l}(\rho_E)\, S^m_l(\mu, \nu) \text{ with } \mathbf{r}_E = (\rho_E, \mu, \nu) \in S_E, \tag{2.6}$$

where the parameters $\sigma^m_{\infty,l}(\rho_E)$ and $p^m_{\infty,l}(\rho_E)$ for $l \geq 0$ and $m = 1, 2, \ldots, 2l+1$ are subject to the exterior conditions, while $S^m_l(\mu,\nu) = E^m_l(\mu)\, E^m_l(\nu)$ are the surface ellipsoidal harmonic functions of degree l and order m, while E^m_l are the Lamé functions of the first kind [8, 10, 20, 26], being regular at the origin.

The aim of the present work is focused on determining the evolution of the exterior boundary S_P of the ellipsoidal tumour. To this due and following [22–24], we assume that the exterior tumour boundary evolves according to the equation

$$\frac{d\mathbf{r}_P}{dt} = -\mu_P \nabla P(\mathbf{r}_P) + \mu_\sigma \nabla\sigma(\mathbf{r}_P) - \mu_\beta \nabla\beta(\mathbf{r}_P) \text{ with } \mathbf{r}_P = (\rho_P, \mu, \nu) \in S_P, \tag{2.7}$$

where μ_P, μ_σ, μ_β are positive proportionality constants that depend on the cells' motility. Equation (2.7) is a modification of the widely used Darcy's law [6, 16, 17, 21, 22, 28], and additionally to the pressure-driven movement, a chemotactic movement of the cell is taken into account, towards the best conditions for the cell's proliferation.

Both the nutrient and the inhibitor agents are governed by the Fick's diffusion law, which allows for diffusion in the direction of less concentration, and are considered to be in a diffusive equilibrium state, due to the relatively small time scale of the diffusion compared to the growth time scale, as can be seen in details in [6, 22]. Their concentrations satisfy the partial differential equations given by

$$\Delta\sigma(\mathbf{r}) = \gamma_j \text{ for every with } \mathbf{r} \in \Omega_j \text{ with } j = N, Q, P, E \tag{2.8}$$

and

$$\Delta\beta(\mathbf{r}) = p_j \text{ for every } \mathbf{r} \in \Omega_j \text{ with } j = N, Q, P, E, \tag{2.9}$$

where each physical constant γ_j and p_j denotes the consumption rate and the production rate, respectively, normalised by the corresponding diffusivity k_σ and k_β, at the corresponding region. Each constant reflects the phase of the biological cycle of the cells occupying the corresponding region. In particular, non-zero values of γ_N support physical considerations on processes aiming to eradicate the nutrient excess, present in the necrotic region, while $\gamma_P \geq \gamma_Q > 0$. Moreover, since cancer cells proliferate much more actively than the normal cells, their metabolic needs are also greater, leading to $\gamma_P \geq \gamma_E \geq 0$. For simplicity and without loss in generality, we additionally assume that $\gamma_E = 0$. Similarly, considering as inhibitor both the metabolic by-products of the living cells and the chemicals produced during necrosis and disintegration, we assume that $p_N \neq 0$ and $p_Q = p_P := p_L$, while it is reasonable to assume that $p_E = 0$.

Additionally, we assume that both the nutrient and the inhibitor concentrations are regular at the centre of the colony and continuous across the tumour's interfaces, as well as their directional derivatives normally to the corresponding interface. For a detailed justification of these regularity assumptions, see [22]. Thus, the boundary conditions that complete the problems regarding the nutrient and the inhibitor concentrations, in terms of the ellipsoidal variables, read as follows,

$$\lim_{\rho \to \rho_j^-} \sigma(\rho, \mu, \nu) = \lim_{\rho \to \rho_j^+} \sigma(\rho, \mu, \nu) \text{ with } j = N, Q, P \tag{2.10}$$

https://doi.org/10.1017/S0956792518000499 Published online by Cambridge University Press

and

$$\lim_{\rho\to\rho_j^-}\beta(\rho,\mu,\nu)=\lim_{\rho\to\rho_j^+}\beta(\rho,\mu,\nu)\text{ with }j=N,Q,P, \tag{2.11}$$

while the nutrient concentration on S_E is dictated by the inhomogeneous exterior data given in (2.5) and the inhibitor concentration is just required to decay in the exterior of the tumour, being eliminated in a comparatively long distance from the colony. Moreover, in terms of the outward unit normal vector $\hat{\boldsymbol{\rho}}$ on each confocal ellipsoidal surface S_j and in view of the well-known ellipsoidal gradient differential operator [8], the ellipsoidal normal derivative on S_j reads as

$$\hat{\boldsymbol{\rho}}\cdot\nabla=\frac{\sqrt{\rho_j^2-h_2^2}\sqrt{\rho_j^2-h_3^2}}{\sqrt{\rho_j^2-\mu^2}\sqrt{\rho_j^2-\nu^2}}\frac{\partial}{\partial\rho}\text{with }\nabla=\frac{\hat{\boldsymbol{\rho}}}{h_\rho(\mathbf{r}_j)}\frac{\partial}{\partial\rho}+\frac{\hat{\boldsymbol{\mu}}}{h_\mu(\mathbf{r}_j)}\frac{\partial}{\partial\mu}+\frac{\hat{\boldsymbol{\nu}}}{h_\nu(\mathbf{r}_j)}\frac{\partial}{\partial\nu}\text{ at }\mathbf{r}_j=(\rho_j,\mu,\nu) \tag{2.12}$$

for every $\mu^2\in\left[h_3^2,h_2^2\right]$ and $\nu^2\in\left[0,h_3^2\right]$ with $j=N,Q,P,E$, where h_ρ, h_μ and h_ν are the ellipsoidal metric coefficients [8, 26]. Therefore, the continuity conditions for the normal derivatives yield

$$\lim_{\rho\to\rho_j^-}\frac{\partial\sigma(\rho,\mu,\nu)}{\partial\rho}=\lim_{\rho\to\rho_j^+}\frac{\partial\sigma(\rho,\mu,\nu)}{\partial\rho}\text{ with }j=N,Q,P \tag{2.13}$$

and

$$\lim_{\rho\to\rho_j^-}\frac{\partial\beta(\rho,\mu,\nu)}{\partial\rho}=\lim_{\rho\to\rho_j^+}\frac{\partial\beta(\rho,\mu,\nu)}{\partial\rho}\text{ with }j=N,Q,P. \tag{2.14}$$

Next, we assume that each cell moves according to the modification of the Darcy law, as introduced in (2.7) and its velocity yields

$$\mathbf{v}(\mathbf{r})=-\mu_P\nabla P(\mathbf{r})+\mu_\sigma\nabla\sigma(\mathbf{r})-\mu_\beta\nabla\beta(\mathbf{r})\text{ with }\mathbf{r}\in\bigcup_{j=N,Q,P,E}\Omega_j. \tag{2.15}$$

Applying the divergence operator on both sides of the velocity field (2.15) and implying (2.8) and (2.9), we obtain the pressure field as

$$\Delta P(\mathbf{r})=F_j\text{ for }\mathbf{r}\in\Omega_j\text{ with }j=N,Q,P,E, \tag{2.16}$$

where

$$F_j:=-G_j/\mu_P+\mu_\sigma\gamma_j/\mu_P-\mu_\beta p_j/\mu_P, \tag{2.17}$$

while $G_j:=\nabla\cdot\mathbf{v}(\mathbf{r}_j)$ denote the mass per unit volume, per unit time, that is produced or lost in the region Ω_j and normalised by the tissue's density [22], while it is considered constant in the corresponding region. Taking into consideration the restrictions on the constants γ_j and p_j, as well as definition (2.17), we deduce that the constants F_N, F_Q, F_P are in general not equal between each other, nor zero and also that $F_E=0$. The conditions assigned to the pressure field demand regularity at the centre of the colony and continuity for both the pressure and its normal derivative across the entire interior to the tumour interfaces, namely

$$\lim_{\rho\to\rho_j^-}P(\rho,\mu,\nu)=\lim_{\rho\to\rho_j^+}P(\rho,\mu,\nu)\text{ for }j=N,Q \tag{2.18}$$

https://doi.org/10.1017/S0956792518000499 Published online by Cambridge University Press

and

$$\lim_{\rho\to\rho_j^-}\frac{\partial P(\rho,\mu,\nu)}{\partial\rho}=\lim_{\rho\to\rho_j^+}\frac{\partial P(\rho,\mu,\nu)}{\partial\rho}\ \text{for}\ j=N,Q,P,E. \tag{2.19}$$

The interfaces S_P and S_E distinguish regions characterised by different densities, since the cancerous mass is in general more dense than the host tissue and the healthy compartment formed around the tumour [7, 17]. Therefore, the corresponding boundary conditions on S_P and S_E are dictated by the Young–Laplace equation for two-face incompressible fluids, namely

$$\lim_{\rho\to\rho_j^-}P(\mathbf{r})-\lim_{\rho\to\rho_j^+}P(\mathbf{r})=a_jJ(\mathbf{r}_j)\ \text{with}\ j=P,E, \tag{2.20}$$

where $J(\mathbf{r}_j)$ stands for the mean curvature at the point $\mathbf{r}_j$ of the ellipsoidal surface, which is given via the expression [8]

$$J(\mathbf{r}_j)=-\frac{1}{2}\frac{\rho_j\sqrt{\rho_j^2-h_3^2}\sqrt{\rho_j^2-h_2^2}}{\sqrt{\rho_j^2-\mu^2}\sqrt{\rho_j^2-\nu^2}}\left(\frac{1}{\rho_j^2-\mu^2}+\frac{1}{\rho_j^2-\nu^2}\right) \tag{2.21}$$

for every $\mu^2\in\left[h_3^2,h_2^2\right]$ and $\nu^2\in\left[0,h_3^2\right]$ with $a_P,a_E\in\mathbb{R}$ being proportionality constants. Since $J(\mathbf{r})$ is a continuous function in the coordinate variables μ,ν, it accepts an ellipsoidal expansion as shown in the following:

$$J(\mathbf{r}_j)=\sum_{l=0}^{\infty}\sum_{m=1}^{2l+1}j_l^m(\rho_j)S_l^m(\mu,\nu)\ \text{with}\ \mathbf{r}_j=(\rho_j,\mu,\nu)\in S_j \tag{2.22}$$

for $j=P,E$, $\mu^2\in\left[h_3^2,h_2^2\right]$ and $\nu^2\in\left[0,h_3^2\right]$. Additionally, on the surface S_E the trace of the exterior pressure is given in the form of (2.6).

The model is completed by combining the solutions of the aforementioned problems in equation (2.7), which determines the velocity of the cells occupying the exterior tumour boundary. In particular, in order for the corresponding problems to be treated analytically, we assume that the ellipsoidal tumour evolves, maintaining its confocality, so that all interfaces are members of the same ellipsoidal system throughout the tumour evolution. Therefore, we assume that the cells move only in the normal direction, a condition secured if $d\mu/dt=0=d\nu/dt$. Consequently, since in the ellipsoidal system we have [8, 9]

$$\frac{d\mathbf{r}}{dt}=\hat{\boldsymbol{\rho}}h_\rho(\mathbf{r})\frac{d\rho}{dt}+\hat{\boldsymbol{\mu}}h_\mu(\mathbf{r})\frac{d\mu}{dt}+\hat{\boldsymbol{\nu}}h_\nu(\mathbf{r})\frac{d\nu}{dt}, \tag{2.23}$$

we deduce that $\hat{\boldsymbol{\rho}}\cdot\frac{d\mathbf{r}}{dt}=h_\rho(\mathbf{r})\frac{d\rho}{dt}$. By means of (2.7) and (2.12) and inserting the metric coefficient

$$h_\rho(\mathbf{r})=\frac{\sqrt{\rho^2-\mu^2}\sqrt{\rho^2-\nu^2}}{\sqrt{\rho^2-h_3^2}\sqrt{\rho^2-h_2^2}}, \tag{2.24}$$

we arrive at

$$h_\rho^2(\mathbf{r}_P)\frac{d\rho_P}{dt}=-\mu_P\frac{dP(\mathbf{r}_P)}{d\rho}+\mu_\sigma\frac{d\sigma(\mathbf{r}_P)}{d\rho}-\mu_\beta\frac{d\beta(\mathbf{r}_P)}{d\rho}\ \text{with}\ \mathbf{r}_P=(\rho_P,\mu,\nu)\in S_P, \tag{2.25}$$

which is an ordinary differential equation – it holds for $\mathbf{r}_P(t)=(\rho_P(t),\mu,\nu)\in S_P$ and it is subject to an initial condition $\rho_P(0)=R_P>h_2$. Once computed, its solution determines the tumour's

https://doi.org/10.1017/S0956792518000499 Published online by Cambridge University Press

exterior boundary evolution. In order for (2.25) to be solved, the pressure, the nutrient concentration and the inhibitor concentration, which are solutions of the corresponding problems, have to be introduced. Therefore, we begin the analysis of the model by solving the problems (2.8), (2.10) and (2.13) for the nutrient concentration, (2.9), (2.11) and (2.14) for the inhibitor concentration and (2.16)–(2.21) for the pressure field. This is the task accomplished in the next section.

Before we proceed though, it is worth reminding that the model described above concerns phenomena that take place in two different scales. Processes that take place in the small scale, as the diffusion of the nutrient and of the inhibitor, appear as if they were static phenomena and thus they are described by means of the elliptic boundary value problems (2.8)–(2.14). The tumour growth occurs in the large time scale and its time dependence is exactly what we are looking for by analysing the model. Therefore, the radial variable in the tumour structure depends on time, a fact reflected on the evolution equation (2.25). This fact justifies that the whole problem developed in this section, in view of the model that we described, is actually a free boundary problem, as the boundaries that define the fundamental regions of the problem are also part of the problem. The existence and stability of such problems for the radially symmetric case have been studied in a series of papers, such as [13] and the references therein.

Since the dependence in time of the diffusion processes is intrinsic and it is inherited via the time dependence of the radial variable $\rho\,(t)$, we solve the corresponding problems as if they were elliptic boundary value problems, temporarily ignoring time, which eventually joins in the fundamental formula of the evolution equation.

3 Analytical solutions of the model's problems

The above problems will be solved by properly applying the standard method of separation of variables in every ellipsoidal compartment Ω_j for $j = N, Q, P, E$. To this end, we remind that the interior ellipsoidal harmonic functions of degree $l \geq 0$ and order $m = 1, 2, ..., 2l + 1$ are given in terms of the corresponding Lamé functions of the first kind $E_l^m(\rho)$ as

$$\mathbb{E}_l^m(\rho, \mu, \nu) = E_l^m(\rho) S_l^m(\mu, \nu), \tag{3.1}$$

where $S_l^m(\mu, \nu) = E_l^m(\mu) E_l^m(\nu)$ are the surface ellipsoidal harmonic functions [8, 10, 20, 26]. Similarly, the exterior ellipsoidal harmonic functions of the same degree and order are given by the product

$$\mathbb{F}_l^m(\rho, \mu, \nu) = F_l^m(\rho) S_l^m(\mu, \nu), \tag{3.2}$$

where $F_l^m(\rho) = (2l + 1) I_l^m(\rho) E_l^m(\rho)$ are the corresponding Lamé functions of the second kind, whilst $I_l^m(\rho)$ stands for the following elliptic integral

$$I_l^m(\rho) = \int_{\rho}^{+\infty} \frac{dt}{(E_l^m(t))^2 \sqrt{t^2 - h_2^2} \sqrt{t^2 - h_3^2}}. \tag{3.3}$$

https://doi.org/10.1017/S0956792518000499 Published online by Cambridge University Press

Here we remind the orthogonality property of the surface ellipsoidal harmonic functions that holds on every ellipsoidal surface S_ρ

$$\iint\limits_{S_\rho} S_l^m(\mu,\nu)S_{l'}^{m'}(\mu,\nu)\frac{ds(\mu,\nu)}{\sqrt{\rho^2-\mu^2}\sqrt{\rho^2-\nu^2}} = \gamma_l^m \delta_{ll'}\delta_{mm'}, \tag{3.4}$$

in view of the Kronecker delta notation, where $ds(\mu,\nu)$ is the ellipsoidal surface element and γ_l^m are the L^2 norm of the surface ellipsoidal harmonic $S_l^m(\mu,\nu)$ [8].

Since each Poisson's partial differential equation, rendered by (2.8), (2.9) and (2.16), has a constant non-homogeneous term, we suggest in a trivial manner (see Appendix A1 for details) that the following function can serve as a particular solution,

$$f_{part,j}(\mathbf{r}) = A_j\rho^2\left[d_0^1E_0^1(\mu)E_0^1(\nu) + d_2^1E_2^1(\mu)E_2^1(\nu) + d_2^2E_2^2(\mu)E_2^2(\nu)\right] \text{ for } j = N, Q, P, E, \tag{3.5}$$

where

$$d_0^1 = \frac{1}{6},\ d_2^1 = -\frac{1}{6\left(\Lambda-\Lambda'\right)\left(\Lambda-\alpha_1^2\right)} \text{ and } d_2^2 = \frac{1}{6\left(\Lambda-\Lambda'\right)\left(\Lambda'-\alpha_1^2\right)}, \tag{3.6}$$

while Λ and Λ' are the roots of the second-degree quadratic equation $\sum_{i=1}^{3}\frac{1}{\Lambda-\alpha_i^2} = 0$ and the constants A_j for $j = N, Q, P, E$ are defined appropriately to match the corresponding equation. For reasons of notational convenience in the forthcoming concrete presentation of our analytical results, we additionally define $d_l^m := 0$ for every $l \geq 1$ and $m = 1, 2, ..., 2l+1$, excluding the non-vanishing values for $(l,m) \neq (2,1)$ and $(l,m) \neq (2,2)$.

Skipping the details of the tedious but straightforward calculations (see Appendix A2), the analytical solutions are obtained in a closed compact fashion in terms of the Heaviside function

$$H(\rho-\rho_j) = \begin{cases} 1, & \rho \geq \rho_j \\ 0, & \rho < \rho_j \end{cases} \text{ with } j = N, Q, P, E, \tag{3.7}$$

using the additional notation for $l = 0, 1, 2, ...$ and $m = 1, 2, ..., 2l+1$ with $\rho \in [h_2, \rho_E)$

$$e_l^m(\rho) = 2E_l^m(\rho) - \rho E_l^{m'}(\rho), \tag{3.8}$$

$$f_l^m(\rho) = -2F_l^m(\rho) + \rho F_l^{m'}(\rho), \tag{3.9}$$

$$R_l^m(\rho) = e_l^m(\rho) + \frac{E_l^m(\rho_E)}{F_l^m(\rho_E)}f_l^m(\rho) \tag{3.10}$$

and also the Wronskian

$$W_l^m(\rho) := W_l^m(E_l^m(\rho), F_l^m(\rho)) = E_l^m(\rho)F_l^{m'}(\rho) - E_l^{m'}(\rho)F_l^m(\rho) \neq 0, \tag{3.11}$$

where the prime denotes differentiation with respect to the argument. Then, the nutrient concentration, which satisfies the problems (2.5), (2.8), (2.10) and (2.13) yields

https://doi.org/10.1017/S0956792518000499 Published online by Cambridge University Press

$$\sigma(\mathbf{r}) = \sum_{l=0}^{\infty}\sum_{m=1}^{2l+1} \Sigma_l^m(\rho)\, S_l^m(\mu,\nu)$$
$$= \sum_{l=0}^{\infty}\sum_{m=1}^{2l+1} \left\{ d_l^m \gamma_N \rho^2 + \left[\sigma_{\infty,l}^m(\rho_E) + d_l^m F_l^m(\rho_E) \left(\left(\gamma_Q - \gamma_N\right)\rho_N \frac{R_l^m(\rho_N)}{W_l^m(\rho_N)} \right.\right.\right.$$
$$\left.\left.\left. - \left(\gamma_Q - \gamma_P\right)\rho_Q \frac{R_l^m(\rho_Q)}{W_l^m(\rho_Q)} - \gamma_P \rho_P \frac{R_l^m(\rho_P)}{W_l^m(\rho_P)} \right) \right] \frac{E_l^m(\rho)}{E_l^m(\rho_E)} \right.$$
$$+ d_l^m \left[H\left(\rho - \rho_N\right)\left(\gamma_Q - \gamma_N\right) \left(\rho^2 - \rho_N \frac{f_l^m(\rho_N) E_l^m(\rho) + e_l^m(\rho_N) F_l^m(\rho)}{W_l^m(\rho_N)} \right) \right.$$
$$- H\left(\rho - \rho_Q\right)\left(\gamma_Q - \gamma_P\right) \left(\rho^2 - \rho_Q \frac{f_l^m(\rho_Q) E_l^m(\rho) + e_l^m(\rho_Q) F_l^m(\rho)}{W_l^m(\rho_Q)} \right)$$
$$\left.\left. - H\left(\rho - \rho_P\right)\gamma_P \left(\rho^2 - \rho_P \frac{f_l^m(\rho_P) E_l^m(\rho) + e_l^m(\rho_P) F_l^m(\rho)}{W_l^m(\rho_P)} \right) \right] \right\} S_l^m(\mu,\nu) \tag{3.12}$$

at any point $\mathbf{r} = (\rho, \mu, \nu)$ with $\rho \in [h_2, \rho_E)$, $\mu^2 \in \left[h_3^2, h_2^2\right]$ and $\nu^2 \in \left[0, h_3^2\right]$. Similarly, for the inhibitor concentration, which is the solution of the problem (2.9), (2.11) and (2.14), we derive

$$\beta(\mathbf{r}) = \sum_{l=0}^{\infty}\sum_{m=1}^{2l+1} B_l^m(\rho) S_l^m(\mu,\nu)$$
$$= \sum_{l=0}^{\infty}\sum_{m=1}^{2l+1} d_l^m \left\{ p_N \rho^2 + F_l^m(\rho_E) \left[\left(p_L - p_N\right)\rho_N \frac{R_l^m(\rho_N)}{W_l^m(\rho_N)} - p_L \rho_P \frac{R_l^m(\rho_P)}{W_l^m(\rho_P)} \right] \frac{E_l^m(\rho)}{E_l^m(\rho_E)} \right.$$
$$+ H\left(\rho - \rho_N\right)\left(p_L - p_N\right) \left(\rho^2 - \rho_N \frac{f_l^m(\rho_N) E_l^m(\rho) + e_l^m(\rho_N) F_l^m(\rho)}{W_l^m(\rho_N)} \right)$$
$$\left. - H\left(\rho - \rho_P\right) p_L \left(\rho^2 - \rho_P \frac{f_l^m(\rho_P) E_l^m(\rho) + e_l^m(\rho_P) F_l^m(\rho)}{W_l^m(\rho_P)} \right) \right\} S_l^m(\mu,\nu) \tag{3.13}$$

for every $\mathbf{r} = (\rho, \mu, \nu)$ with $\rho \in [h_2, \rho_E)$, $\mu^2 \in \left[h_3^2, h_2^2\right]$ and $\nu^2 \in \left[0, h_3^2\right]$. Finally, the pressure field proves to be quite more involved, mainly due to the Young–Laplace conditions (2.20) that need to be satisfied. Nevertheless, the involvement concerns only the coefficients, while the pressure assumes a similar functional form like (3.12) and (3.13), reflecting the similarity in the corresponding boundary value problems. Therein, this field admits

$$P(\mathbf{r}) = \sum_{l=0}^{\infty}\sum_{m=1}^{2l+1} \Pi_l^m(\rho)\, S_l^m(\mu,\nu) = \sum_{l=0}^{\infty}\sum_{m=1}^{2l+1} \left\{ d_l^m F_N \rho^2 \right.$$
$$+ \left[p_{\infty,l}^m(\rho_E) + a_E j_l^m(\rho_E) + a_P j_l^m(\rho_P) \frac{E_l^m(\rho_E) F_l^{m'}(\rho_P) - F_l^m(\rho_E) E_l^{m'}(\rho_P)}{W_l^m(\rho_P)} + d_l^m F_l^m(\rho_E) \right.$$
$$\left. \times \left(\left(F_Q - F_N\right)\rho_N \frac{R_l^m(\rho_N)}{W_l^m(\rho_N)} + \left(F_P - F_Q\right)\rho_Q \frac{R_l^m(\rho_Q)}{W_l^m(\rho_Q)} - F_P \rho_P \frac{R_l^m(\rho_P)}{W_l^m(\rho_P)} \right) \right] \frac{E_l^m(\rho)}{E_l^m(\rho_E)}$$
$$+ d_l^m \left[H\left(\rho - \rho_N\right)\left(F_Q - F_N\right) \left(\rho^2 - \rho_N \frac{f_l^m(\rho_N) E_l^m(\rho) + e_l^m(\rho_N) F_l^m(\rho)}{W_l^m(\rho_N)} \right) \right.$$

https://doi.org/10.1017/S0956792518000499 Published online by Cambridge University Press

$$+H\left(\rho-\rho_Q\right)\left(F_P-F_Q\right)\left(\rho^2-\rho_Q\frac{f_l^m(\rho_Q)\,E_l^m(\rho)+e_l^m(\rho_Q)\,F_l^m(\rho)}{W_l^m(\rho_Q)}\right)$$

$$-H\left(\rho-\rho_P\right)F_P\left(\rho^2-\rho_P\frac{f_l^m(\rho_P)\,E_l^m(\rho)+e_l^m(\rho_P)\,F_l^m(\rho)}{W_l^m(\rho_P)}\right)\Bigg]$$

$$-H\left(\rho-\rho_P\right)a_P j_l^m(\rho_P)\,\frac{E_l^m(\rho)\,F_l^{m'}(\rho_P)-F_l^m(\rho)\,E_l^{m'}(\rho_P)}{W_l^m(\rho_P)}\Bigg\}\,S_l^m(\mu,\nu) \tag{3.14}$$

again for every $\mathbf{r}=(\rho,\mu,\nu)$ with $\rho\in[h_2,\rho_E)$, $\mu^2\in\left[h_3^2,h_2^2\right]$ and $\nu^2\in\left[0,h_3^2\right]$.

Herein, we have to comment on the characterisation implied in the tumour interfaces, by the forms (3.12)–(3.14). It is clear that all fields are point dependent with the angular dependence to persist also on each ellipsoidal surface inside the tumour's structure, which corresponds to any constant value of the radial variable $\rho\in[h_2,\rho_P)$. Therefore, the critical values of the nutrient, σ_N^*, σ_Q^* and also of the inhibitor β^* cannot be met via (3.12) and (3.13), respectively, identifying accordingly all points of each interface S_j with $j=N,Q$. This identification appears natural in the spherical tumour model as the radial symmetry is reflected on the functional forms of $\sigma(\mathbf{r})$ and $\beta(\mathbf{r})$ which depend only on the distance from the centre of the tumour. A physical way out of this puzzle is to consider the ellipsoidal interfaces as ideal surfaces, which distinguish the tumour compartments geometrically, whereas the material interfaces are defined as the locus of the points, which attribute the constant critical values. In this view, we consider the critical values as average values of the corresponding substance on each ellipsoidal surface, obtained by integrating accordingly on the corresponding surface. Thus, via integration of (3.12) on S_N and using the orthogonality property (3.4), we obtain

$$6\sigma_N^*=6\sigma_{\infty,0}^1\left(\rho_E\right)+\gamma_N\rho_N^2+\left(\gamma_Q-\gamma_N\right)\rho_N\left(\rho_N+2\frac{F_0^1(\rho_E)-F_0^1(\rho_N)}{F_0^{1'}(\rho_N)}\right)$$

$$-\left(\gamma_Q-\gamma_P\right)\rho_Q\left(\rho_Q+2\frac{F_0^1(\rho_E)-F_0^1(\rho_Q)}{F_0^{1'}(\rho_Q)}\right)-\gamma_P\rho_P\left(\rho_P+2\frac{F_0^1(\rho_E)-F_0^1(\rho_P)}{F_0^{1'}(\rho_P)}\right), \tag{3.15}$$

while similarly by integrating over S_Q and by means of (3.15), we take

$$6\sigma_Q^*=6\sigma_N^*+\left(\gamma_Q-\gamma_N\right)\left(\rho_Q^2-\rho_N^2+2\rho_N\frac{F_0^1(\rho_N)-F_0^1(\rho_Q)}{F_0^{1'}(\rho_N)}\right) \tag{3.16}$$

and finally, integrating (3.13) over S_Q, we arrive at

$$6\beta^*=p_L\left(\rho_Q^2-\rho_P^2+2\rho_P\frac{F_0^1(\rho_P)-F_0^1(\rho_E)}{F_0^{1'}(\rho_P)}\right)-2\left(p_L-p_N\right)\rho_N\frac{F_0^1(\rho_Q)-F_0^1(\rho_E)}{F_0^{1'}(\rho_N)}. \tag{3.17}$$

Relations (3.15)–(3.17) will be proved very useful in solving the evolution equation in the next section, since they provide interconnections between ρ_N, ρ_Q, ρ_P and ρ_E, which reflects the fact that each interface inherits its growth rate to the others. In other words, this is consistent with the consideration of the tumour as an incompressible fluid which grows without interior holes or deformations during its evolution.

https://doi.org/10.1017/S0956792518000499 Published online by Cambridge University Press

We turn now to the elaboration of the basic equation of this work, which is the evolution equation (2.25). By expanding the function $h_\rho^2(\rho_P, \mu, \nu)$ in terms of surface ellipsoidal harmonics, we obtain

$$h_\rho^2(\rho_P, \mu, \nu) = \frac{E_2^1(\rho_P)\, E_2^2(\rho_P)}{\left(\rho_P^2 - h_3^2\right)\left(\rho_P^2 - h_2^2\right)} \left[S_0^1(\mu, \nu) - \frac{S_2^1(\mu, \nu)}{\left(\Lambda - \Lambda'\right) E_2^1(\rho_P)} + \frac{S_2^2(\mu, \nu)}{\left(\Lambda - \Lambda'\right) E_2^2(\rho_P)} \right]. \tag{3.18}$$

At this point, we insert (3.18), as well as the results (3.12)–(3.14), calculated for $\rho = \rho_P$, into (2.25) we multiply by $S_{l'}^{m'}(\mu, \nu)$ for $l' = 0, 1, 2, \ldots$ and $m' = 1, 2, \ldots, 2l' + 1$ and we integrate over the surface S_P. Due to the orthogonality (3.4), we arrive at a sequence of equations that all involve the rate $\frac{d\rho_P}{dt}$. In particular, by multiplying with $S_0^1(\mu, \nu)$ (for $l = 0$ and $m = 1$) and integrating over S_P, we have

$$\begin{aligned} \frac{d\rho_P}{dt} = & \frac{\left(\rho_P^2 - h_3^2\right)\left(\rho_P^2 - h_2^2\right)}{3E_2^1(\rho_P)\, E_2^2(\rho_P)} \\ & \times \left\{ \left[\mu_\sigma \left(\gamma_Q - \gamma_N\right) - \mu_\beta \left(p_L - p_N\right) - \mu_P \left(F_Q - F_N\right)\right] \left(\rho_P - \rho_N \frac{F_0^{1'}(\rho_P)}{F_0^{1'}(\rho_N)} \right) \right. \\ & \left. + \left[\mu_\sigma \left(\gamma_P - \gamma_Q\right) - \mu_P \left(F_P - F_Q\right)\right] \left(\rho_P - \rho_Q \frac{F_0^{1'}(\rho_P)}{F_0^{1'}(\rho_Q)} \right) - \left(-\mu_\sigma \gamma_N + \mu_\beta p_N + \mu_P F_N\right) \rho_P \right\}, \end{aligned} \tag{3.19}$$

while by using the orthogonality property of $S_l^m(\mu, \nu)$, with $l \in \mathbb{N}^*$ and $m = 1, 2, \ldots, 2l + 1$, where by virtue of the Kronecker delta, we obtain

$$\begin{aligned} & \frac{E_2^1(\rho_P)\, E_2^2(\rho_P)}{\left(\Lambda - \Lambda'\right)\left(\rho_P^2 - h_3^2\right)\left(\rho_P^2 - h_2^2\right)} \left(\frac{\delta_{l2}\delta_{m2}}{E_2^2(\rho_P)} - \frac{\delta_{l2}\delta_{m1}}{E_2^1(\rho_P)} \right) \frac{d\rho_P}{dt} \\ & \quad = -\mu_P \Pi_l^{m'}(\rho_P) + \mu_\sigma \Sigma_l^{m'}(\rho_P) - \mu_\beta \mathrm{B}_l^{m'}(\rho_P), \end{aligned} \tag{3.20}$$

wherein (3.19) may be inserted. On the other hand, the functions $\Pi_l^m(\rho_P)$, $\Sigma_l^m(\rho_P)$ and $\mathrm{B}_l^m(\rho_P)$ are the coefficients of $S_l^m(\mu, \nu)$ in the ellipsoidal expansions of $P(\mathbf{r})$, $\sigma(\mathbf{r})$ and $\beta(\mathbf{r})$ given in (3.14), (3.12) and (3.13), respectively, at the specific point $\mathbf{r} = \mathbf{r}_P = (\rho_P, \mu, \nu)$ and we recall that the prime denotes differentiation with respect to the argument. Relationship (3.19) comprises the evolution equation, while (3.20) stands for the compatibility condition, which must be readily secured. Furthermore, equation (3.20) splits to the following two independent restrictions, i.e.

$$-\mu_P \Pi_l^{m'}(\rho_P) + \mu_\sigma \Sigma_l^{m'}(\rho_P) - \mu_\beta B_l^{m'}(\rho_P) = 0, \tag{3.21}$$

when $l > 0$ and $m = 1, 2, \ldots, 2l + 1$ but $(l, m) \notin \{(2, 1), (2, 2)\}$, while for $l = 2$, $m = 1$ and $l = 2$, $m = 2$, we readily obtain

$$\begin{aligned} & -\mu_P \left(\Pi_2^{2'}(\rho_P) + \frac{E_2^1(\rho_P)}{E_2^2(\rho_P)} \Pi_2^{1'}(\rho_P) \right) + \mu_\sigma \left(\Sigma_2^{2'}(\rho_P) + \frac{E_2^1(\rho_P)}{E_2^2(\rho_P)} \Sigma_2^{1'}(\rho_P) \right) \\ & -\mu_\beta \left(\mathrm{B}_2^{2'}(\rho_P) + \frac{E_2^1(\rho_P)}{E_2^2(\rho_P)} \mathrm{B}_2^{1'}(\rho_P) \right) = 0. \end{aligned} \tag{3.22}$$

https://doi.org/10.1017/S0956792518000499 Published online by Cambridge University Press

The latter is a consequence of the division by parts of the initial relation (3.20), written for $(l, m) = (2,1)$ and for $(l, m) = (2,2)$ in order to eliminate the term $\frac{d\rho_P}{dt}$. On the other hand, both (3.21) and (3.22) need to specify the coefficients of the mean curvature (2.21), entered into expansion (2.22), whereas in view of the orthogonality relation (3.4), they admit

$$j_l^m(\rho_j) = \frac{1}{\gamma_l^m} \iint\limits_{S_{\rho_j}} S_l^m(\mu, \nu) J(\rho_j, \mu, \nu) \frac{ds(\mu, \nu)}{\sqrt{\rho_j^2 - \mu^2}\sqrt{\rho_j^2 - \nu^2}} \text{ with } j = P, E \tag{3.23}$$

for every $l \geq 0$ and $m = 1, 2, \ldots, 2l + 1$.

As can be seen from (3.21) and (3.22), in view of (3.12) and (3.14), the system of equations described by (3.20) implies restrictions between the nutrient supply and the pressure field imposed by the tumour's surrounding medium, as dictated in (2.5) and (2.6), respectively. Thus, it is clear that a tumour will exhibit such ellipsoidal growth only if the nutrient supply responds to the pressure imposed in accordance with equation (3.20) or equivalently with (3.21) and (3.22). This remark is important, as both ellipsoidal tumours do appear *in vivo*, for example in soft tissues as in breast cancer [5] and also because a response of the nutrient supply to the environment's pressure may suggest vascularisation of the tumour.

Equation (3.19), on the other hand, offers the nonlinear ordinary differential equation that determines the evolution of the ellipsoidal tumour boundary S_P, with respect to all the other boundaries, S_N, S_Q and S_E, which synchronously evolve. Thanks to equations (3.15)–(3.17), their evolution is coupled to the evolution of S_P, as can be seen, for example, in (3.16), which provides ρ_Q as a function of ρ_N and in (3.17) which couples them with ρ_P, while equation (3.15) provides ρ_E with respect to ρ_N, ρ_Q and ρ_P. Introducing these functions into (3.19) results in a very intricate nonlinear ordinary differential equation, demanding numerical aid for its solution. The uniqueness of its solution is secured by the initial condition $\rho_P(0) = R_P > h_2$, which corresponds to the exterior boundary of the ellipsoidal tumour at the time that it was initially observed. The task of implementing numerically the solution of (3.19) will be accomplished in Section 5. Before that, it is worth to provide the necessary tools for reducing the above results to more degenerate models, a process that leads to recovering the results obtained from the spheroidal models [18, 23, 24] and also from the spherical models [6, 17, 22].

4 Reduction to degenerate geometries

The strict inequalities $0 < \alpha_3 < \alpha_2 < \alpha_1 < +\infty$ form the basic reason why the triaxial ellipsoid reflects the general geometric anisotropy of the 3D space. As it is well known, the reduction of general results from the ellipsoidal to the spheroidal or to the spherical geometry is not straightforward, since certain indeterminacies appear during the limiting process. This is due to the fact that the spherical system springs from a zero-dimensional manifold, i.e. the centre, while the ellipsoidal system springs from a 2D manifold, i.e. the focal ellipse.

The equality of two out of three axes within (4.1) causes the degeneration of an ellipsoid to a spheroid, whose axis of symmetry coincides with the third axis. More specific, a prolate spheroid can be obtained whenever $0 < \alpha_3 = \alpha_2 < \alpha_1 < +\infty$, while an oblate spheroid corresponds to $0 < \alpha_3 < \alpha_2 = \alpha_1 < +\infty$, where the axis of symmetry is the x_1-axis for the prolate spheroid and the x_3-axis for the oblate spheroid. The interesting asymptotic case of the needle can be reached by a prolate spheroid whenever we have $0 < \alpha_3 = \alpha_2 \ll \alpha_1 < +\infty$, whilst in the case where

https://doi.org/10.1017/S0956792518000499 Published online by Cambridge University Press

$0 < \alpha_3 \ll \alpha_2 = \alpha_1 < +\infty$, the oblate spheroid takes the shape of a circular disc. As far as the semi-focal distances are concerned, we have that $h_1 = 0$ and $h_2 = h_3 = c$ with $c > 0$ for the case of a prolate spheroid with semi-focal distance c, while $h_3 = 0$ and $h_1 = h_2 = \bar{c}$ with $\bar{c} > 0$ for the case of an oblate spheroid with semi-focal distance $\bar{c}$. The simple transformation $c \to -i\bar{c}$ with $c, \bar{c} > 0$ allows the transition from the prolate to the oblate spheroid, while the replacement $\bar{c} \to ic$ with $c, \bar{c} > 0$ secures the converse. In terms of $1 \leq \tau := \cosh\eta < +\infty$, $-1 \leq \zeta := \cos\theta \leq 1$ and $\varphi \in [0, 2\pi)$ for the prolate spheroid, the corresponding results for the oblate spheroid can be obtained through $\tau \to i\lambda$ with $1 \leq \tau < +\infty$, where $0 \leq \lambda := \sinh\eta < +\infty$ is the characteristic variable of the oblate system. Obviously, the inverse transformation $\lambda \to -i\tau$ with $0 \leq \lambda < +\infty$ leads to the converse result. Consequently, from this point on we shall refer to the prolate spheroidal geometry, since the oblate spheroidal geometry is recovered via

$$\tau \to i\lambda \text{ and } c \to -i\bar{c}. \tag{4.1}$$

In terms of the unit normal vector $\hat{\boldsymbol{\tau}}$ for the prolate spheroidal coordinates, the ellipsoidal variables are connected with the corresponding prolate spheroidal ones by

$$\rho = c\tau \text{ and } \hat{\boldsymbol{\rho}} \to \hat{\boldsymbol{\tau}}, \text{where } \rho \in [h_2, +\infty) \text{ with } 1 \leq \tau < +\infty, \tag{4.2}$$

while

$$\frac{\mu\nu}{h_2 h_3} = \zeta, \tag{4.3}$$

$$\frac{\sqrt{\mu^2 - h_3^2}\sqrt{h_3^2 - \nu^2}}{h_1 h_3} = \sqrt{1 - \zeta^2}\cos\varphi \tag{4.4}$$

and

$$\frac{\sqrt{h_2^2 - \mu^2}\sqrt{h_2^2 - \nu^2}}{h_1 h_2} = \sqrt{1 - \zeta^2}\sin\varphi, \tag{4.5}$$

whereas $\mu^2 \in \left[h_3^2, h_2^2\right]$, $\nu^2 \in \left[0, h_3^2\right]$ and $1 \leq \tau < +\infty$, $\varphi \in [0, 2\pi)$. For $\alpha_2 = \alpha_3$ (prolate spheroid) the constants appearing within (3.6) yield $\lim\limits_{\alpha_2 \to \alpha_3} \Lambda = \frac{2\alpha_1^2 + \alpha_2^2}{3}$ and $\lim\limits_{\alpha_2 \to \alpha_3} \Lambda' = \alpha_2^2$. On the other hand, the elliptic integrals (3.3) in prolate spheroidal geometry ($\alpha_2 = \alpha_3$) read as

$$\lim_{\alpha_2 \to \alpha_3} I_l^m(\rho) = \int_{\rho}^{+\infty} \frac{dt}{\left[\lim\limits_{\alpha_2 \to \alpha_3} E_l^m(t)\right]^2 \left(t^2 - \alpha_1^2 + \alpha_2^2\right)} \text{ for } \rho \in [h_2, +\infty) \tag{4.6}$$

for $l \geq 0$ and $m = 1, 2, \ldots, 2l + 1$ and they are no more elliptic, while they can be evaluated with analytic manipulations. Specifically, the determination of $I_0^1(\rho)$ demands the calculation of the corresponding integral (4.6) for $l = 0$ and $m = 1$ in terms of the variable τ, i.e.

$$\lim_{\alpha_2 \to \alpha_3} I_0^1(\rho) = \frac{1}{2c} \ln \frac{\tau + 1}{\tau - 1} \text{ for } \rho \in [h_2, +\infty) \text{ with } 1 \leq \tau < +\infty \text{ and } c > 0. \tag{4.7}$$

The other elliptic integrals, which concern the exterior ellipsoidal harmonic eigenfunctions for degree $l \geq 1$ and order $m = 1, 2, \ldots, 2l + 1$, are given explicitly in terms of the $\lim\limits_{\alpha_2 \to \alpha_3} I_0^1(\rho)$ in

https://doi.org/10.1017/S0956792518000499 Published online by Cambridge University Press

their prolate spheroidal expressions for $\alpha_2 = \alpha_3$. As far as the interior solid ellipsoidal harmonics is concerned, their Cartesian representation implies easily a relative reduction procedure, even though only few ellipsoidal harmonics are given in closed compact fashion. Finally, the limiting cases of the needle and of the disc are asymptotic reductions of the prolate and the oblate spheroidal geometry, respectively. Therefore, for the needle we obtain $\alpha_1/\alpha_2 = \tau/\sqrt{\tau^2-1} \to +\infty$, where $1 \leq \tau < +\infty$ and for the disc we arrive at the limiting condition $\alpha_3/\alpha_2 = \lambda/\sqrt{\lambda^2+1} \to 0^+$, where $0 \leq \lambda < +\infty$.

If we change our perspective and demand to reduce our results to the spherical case, where the complete isotropy of the 3D space is considered, we proceed as follows. The sphere corresponds to $\alpha_1 = \alpha_2 = \alpha_3 = \alpha$, where α is the radius of the sphere, where the reference ellipsoid reduces. In this case, $h_\kappa = 0$ for $\kappa = 1, 2, 3$, which means that all the semi-focal distances of the ellipsoid coincide at the origin. Defining the limit from the ellipsoid to the sphere as '$\lim\limits_{e\to s}$', the constants into (3.6) give $\lim\limits_{e\to s} \Lambda = \lim\limits_{e\to s} \Lambda' = \alpha^2$. The intervals of variation of the variables μ and ν imply that in this particular case $\lim\limits_{e\to s} \mu = \lim\limits_{e\to s} \nu = 0$ for $\kappa = 1, 2, 3$. In terms of the unit normal vector $\hat{\mathbf{r}}$ of the spherical coordinate system, the connection between the ellipsoidal variables and the corresponding spherical ones $r \geq 0$, $-1 \leq \zeta := \cos\theta \leq 1$ and $\varphi \in [0, 2\pi)$ is met by

$$\lim_{e\to s} \rho = \lim_{e\to s} \left(\sqrt{\rho^2 - h_2^2} \right) = \lim_{e\to s} \left(\sqrt{\rho^2 - h_3^2} \right) = r \text{ and } \hat{\boldsymbol{\rho}} \to \hat{\mathbf{r}} \text{ where } \rho \in [h_2, +\infty) \text{ with } r \geq 0 \tag{4.8}$$

for the radial component and, as previously,

$$\frac{\mu\nu}{h_2 h_3} = \zeta, \quad \frac{\sqrt{\mu^2 - h_3^2}\sqrt{h_3^2 - \nu^2}}{h_1 h_3} = \sqrt{1-\zeta^2}\cos\varphi \text{ and } \frac{\sqrt{h_2^2 - \mu^2}\sqrt{h_2^2 - \nu^2}}{h_1 h_2} = \sqrt{1-\zeta^2}\sin\varphi, \tag{4.9}$$

for the angular dependence. The elliptic integrals (3.3) assume the values

$$\lim_{e\to s} I_l^m(\rho) = \frac{1}{(2l+1)\, r^{2l+1}}, \tag{4.10}$$

where $l \geq 0$ and $m = 1, 2, \ldots, 2l+1$ for every $\rho \in [h_2, +\infty)$ and $r \geq 0$.

By virtue of the previous analysis about the reduction rules to the spheroidal (relations (4.1)–(4.7)) or to the spherical (expressions (4.8)–(4.10)) geometry, the manipulation of our main results for the nutrient concentration (3.12), the inhibitor concentration (3.13), the pressure field (3.14), the relationships for the critical values (3.15)–(3.17) and the evolution equation (3.19) is a straightforward task and leads to recovering the corresponding and already known results from the literature [22–24].

5 Numerical implementation

The ellipsoidal coordinate system provides the appropriate means for solving classical boundary value problems involving cancerous tumour growth. However, this is amenable to analytical techniques and provides closed form exact solutions only if we impose particular conditions as already discussed extensively in the previous sections or if we work within the frame of simple orthogonal geometries. Hence, as a fair approximation to real-life situations, we adopt this genuine 3D system that reflects the complete geometrical anisotropy of the 3D space to obtain

https://doi.org/10.1017/S0956792518000499 Published online by Cambridge University Press

analytical results for the corresponding fields, i.e. the nutrient (3.12), the inhibitor (3.13) and the pressure (3.14). We emphasise here that we do not refer to the anisotropy imposed by the physical characteristics of the phenomenon under consideration, which, for the purpose of the present work, we choose to restrict to the simplest description of the piecewise isotropic characteristics. Therefore, we refer to a geometrically anisotropic model, while the model equations in each compartment are isotropic.

Nevertheless, fully analytical solutions do not always meet the required accuracy or it is difficult to be manipulated numerically. Even in simple geometries as the spherical, the spheroidal or the ellipsoidal one whereas the Laplace's and the Poisson's partial differential equations admit standard separation of variables, the semi-analytical approach is inherited. Indeed, the ordinary differential equation describing the evolution of the tumour's exterior boundary (3.19) is highly nonlinear and its solution needs numerical implementation. To this purpose, there is always room for pure numerical analysis or better for sophisticated computational treatment of our analytical results. Under this useful aspect, we inherit the semi-analytical attribute to our method, in order to validate the behaviour of our analytical formulae and predict the evolution in time of the tumour under the physical constraints (3.21) and (3.22), as well as the helpful critical conditions (3.15)–(3.17).

In view of the numerical treatment of the aforementioned fields, the values for the parameters and constants involved are mostly taken from the bibliography [2, 3, 5, 6, 16, 17, 21, 30]. Initially, we assume an ellipsoidal system which springs out from a given and fixed triaxial reference ellipsoid (2.1) with basic semi-axis $\alpha_1 = 0.9 \times 10^{-2}$ m, $\alpha_2 = 0.6 \times 10^{-2}$ m and $\alpha_3 = 0.4 \times 10^{-2}$ m, providing the related semi-focal distances $h_1 = 0.447 \times 10^{-2}$ m, $h_2 = 0.806 \times 10^{-2}$ m and $h_3 = 0.671 \times 10^{-2}$ m. Next, we confine the boundaries of the compartments of the tumour with respect to the 'radial' ellipsoidal variable $\rho \in [h_2, \rho_E)$ [=] m (note that $\mu \in [h_3, h_2]$ and $\nu \in [-h_3, h_3]$). To achieve that, we inherit the behaviour of the already examined symmetric models for sphere-type and spheroidal-type tumours [24]. Specifically, for the complete isotropic case and in order to evaluate ρ_N, ρ_Q, ρ_P and ρ_E, we assume that an ellipsoidal and a spherical tumour occupy approximately the same space, hence their volumes must be equal, i.e. $V_S = V_E$ or equivalently saying $r_j^3 = \rho_j \sqrt{\rho_j^2 - h_3^2} \sqrt{\rho_j^2 - h_2^2}$ for $j = N, Q, P, E$, which a solvable equation for each boundary ρ_j, when the corresponding spherical radii r_j are known. A typical set of spherical boundary values that are taken from [24] represent the standard geometrical structure of a tumour, those being $r_N = 0.647 \times 10^{-2}$ m, $r_Q = 0.763 \times 10^{-2}$ m, $r_P = 0.851 \times 10^{-2}$ m and $r_E = 0.987 \times 10^{-2}$ m. They lead to the equivalent ellipsoidal variables, by solving the cubic equation with respect to ρ_j^2 and choosing the real solutions that satisfy the sequence of inequalities $\rho_E > \rho_P > \rho_Q > \rho_N > h_2$, those being met by the values $\rho_N = 0.927 \times 10^{-2}$ m, $\rho_Q = 1.002 \times 10^{-2}$ m, $\rho_P = 1.066 \times 10^{-2}$ m and $\rho_E = 1.173 \times 10^{-2}$ m, all above referring to the equilibrium state sizes of the tumour's compartments.

In the sequel, we provide the necessary physical parameters that appear in every involved quantity. Therein, for the nutrient field σ[=] kg/m^3 we use $\gamma_N = 5$ kg/m^5, $\gamma_Q = 20$ kg/m^5 and $\gamma_P = 50$ kg/m^5, for the inhibitor field β[=] kg/m^3 we insert $p_N = -40$ kg/m^5 and $p_L = -20$ kg/m^5, while for the pressure field P [=] kg/ms^2 we assume that $F_N = 20$ kg/m^{3}s^2, $F_Q = 30$ kg/m^{3}s^2 and $F_P = 40$ kg/m^{3}s^2, as well as the constants $\alpha_E = 1.4 \times 10^{-6}$ kg/s^2 and $\alpha_P = 1.0 \times 10^{-6}$ kg/s^2. A detailed dimensionless analysis secures the validity of the aforementioned values, which is verified by the proper behaviour of the corresponding fields given below. Additionally,

https://doi.org/10.1017/S0956792518000499 Published online by Cambridge University Press

with respect to the parameters $\sigma^m_{\infty,l}(\rho_E)$ and $p^m_{\infty,l}(\rho_E)$ for $l \geq 0$ and $m = 1, 2, \ldots, 2l+1$, which are subject to the exterior conditions (2.5) and (2.6), respectively, we deal with two different cases. The first one refers to the application of a constant pressure $p^1_{\infty,0}(\rho_E) = 15 \times 10^{-4}\,\mathrm{kg/ms^2}$ and the use of the full expansion (2.5) for the nutrient external supply, where the first term is $\sigma^1_{\infty,0}(\rho_E) = 2.5 \times 10^{-4}\,\mathrm{kg/m^3}$. The second situation refers to an exterior constant nutrient concentration $\sigma^1_{\infty,0}(\rho_E) = 2.5 \times 10^{-4}\,\mathrm{kg/m^3}$ and the utilisation of the complete series (2.6) for the exterior pressure, where the first term is $p^1_{\infty,0}(\rho_E) = 15 \times 10^{-4}\,\mathrm{kg/ms^2}$. These values in both cases are arbitrarily chosen without loss of generality and comprise the first terms of the series expansions (2.5) and (2.6). Once we imply $\sigma^1_{\infty,0}(\rho_E) = 2.5 \times 10^{-4}\,\mathrm{kg/m^3}$, then the critical values of the nutrient and the inhibitor fields are directly derived from (3.15)–(3.17) as $\sigma^*_N = 1.25 \times 10^{-4}\,\mathrm{kg/m^3}$, $\sigma^*_Q = 1.4 \times 10^{-4}\,\mathrm{kg/m^3}$ and $\beta^* = 1.6 \times 10^{-4}\,\mathrm{kg/m^3}$, respectively. Next, for the evaluation of the physical proportionality parameters μ_P, μ_σ and μ_β that reflect the cells motility into the evolution equation (3.19), we demand such values so as to sustain a steady state for the physical system, by imposing the equilibrium state condition $\frac{d\rho_P}{dt} = 0$ within relation (3.19) and requiring μ_P, μ_σ and μ_β to satisfy such equality for the choice of ρ_N, ρ_Q, ρ_P and ρ_E defined earlier. This procedure leads to the choice of $\mu_P = 1.33 \times 10^{-6}\,\mathrm{m^3 s/kg}$, $\mu_\sigma = 6.77 \times 10^{-7}\,\mathrm{m^5/kgs}$ and $\mu_\beta = 8.04 \times 10^{-7}\mathrm{m^5/kgs}$. Finally, the coefficients $j^m_l(\rho_j)$ of the mean curvature (2.21) defined in (2.22), for every $l \geq 0$ and $m = 1, 2, \ldots, 2l+1$ at $\mathbf{r}_j = (\rho_j, \mu, \nu) \in S_j$ with $j = P, E$, are provided via the integral (3.23).

Consequently, we are now ready to provide plots, concerning the equilibrium state, for the nutrient and the inhibitor concentrations, as well as for the pressure field, given via the derived analytical expressions (3.12)–(3.14), respectively, considering either constant pressure or constant nutrient concentration on the exterior boundary $\rho = \rho_E$, as discussed earlier. To do so, we evaluate the series terms up to a certain order of the ellipsoidal harmonic eigenfunctions, until convergence is obtained. Therein, the expansions are taken for $l = 0, 1, 2, \ldots, M$, M being sufficiently large to obtain the desired accuracy, while $m = 1, 2, \ldots, 2l+1$. This computational work is based on the proper numerical calculation of ellipsoidal harmonics of any order [8], which is the key method for the implementation of the analytical results. Besides, physical parameters or characteristics secure the sufficient determination of this upper limit M, depending on the kind of exterior fields $\sigma_\infty(\mathbf{r}_E)$ and $\mathrm{P}_\infty(\mathbf{r}_E)$ with $\mathbf{r}_E = (\rho_E, \mu, \nu)$, as well as on the assumed Young–Laplace equation's constants, etc. Additionally, we note that all calculations are compatible with the two main independent restrictions, imposed by relationships (3.21) and (3.22).

First we examine the circumstance of imposing a constant pressure $p^1_{\infty,0}(\rho_E) = 15 \times 10^{-4}\,\mathrm{kg/ms^2}$ on the tumour's exterior boundary, whereas $p^m_{\infty,l}(\rho_E) = 0$ for $l \geq 1$ and $m = 1, 2, \ldots, 2l+1$. From the compatibility relationships (3.21) and (3.22), we calculate the coefficients of the nutrient's concentration onto $\rho = \rho_E$ from (2.5), i.e. $\sigma^m_{\infty,l}(\rho_E)$ for $l \geq 0$ (up to $l = 10$) and $m = 1, 2, \ldots, 2l+1$, additionally to the case $l = 0$ and $m = 1$, where, as we have discussed earlier, $\sigma^1_{\infty,0}(\rho_E) = 2.5 \times 10^{-4}\,\mathrm{kg/m^3}$. The numerical experiments have shown that the values of σ and P become stable for $l = l_{\max} \equiv M = 4$ (note that actually β in (3.13) does not involve infinite series expansion but a finite expression). Also, it is readily observed that by setting smaller values of the implicated constants in the Young–Laplace equation (2.20), e.g. $\alpha_E = 0.2 \times 10^{-6}\,\mathrm{kg/s^2}$ and $\alpha_P = 0.2 \times 10^{-6}\,\mathrm{kg/s^2}$, then convergence is obtained almost immediately for $l = l_{\max} \equiv M = 2$. In Table 1, we present the nutrient's supply coefficients $\sigma^m_{\infty,l}(\rho_E)$ up to the critical $l = 4$ ($m = 1, 2, \ldots, 2l+1$).

https://doi.org/10.1017/S0956792518000499 Published online by Cambridge University Press

Table 1. *The coefficients of the nutrient's exterior supply* $\sigma^m_{\infty,l}(\rho_E)$ *up to* $l=4$ $(m=1,2,\ldots,2l+1)$ $(10^{-4}\text{kg/m}^{2l+3})$

	l				
m	0	1	2	3	4
1	$2.50000\times10^{+00}$	-1.37307×10^{-12}	$-1.33686\times10^{+01}$	1.48132×10^{-11}	$-5.22043\times10^{+01}$
2		2.31318×10^{-18}	$2.00456\times10^{+01}$	-6.77570×10^{-12}	$1.15506\times10^{+02}$
3		2.80091×10^{-19}	1.85615×10^{-18}	1.01594×10^{-18}	$-7.30038\times10^{+01}$
4			-5.24876×10^{-20}	-3.19852×10^{-20}	-1.77154×10^{-19}
5			-1.90069×10^{-19}	-2.39349×10^{-19}	1.18059×10^{-19}
6				-3.61413×10^{-19}	2.98807×10^{-20}
7				2.27508×10^{-19}	1.83067×10^{-18}
8					-1.41602×10^{-20}
9					4.70412×10^{-21}

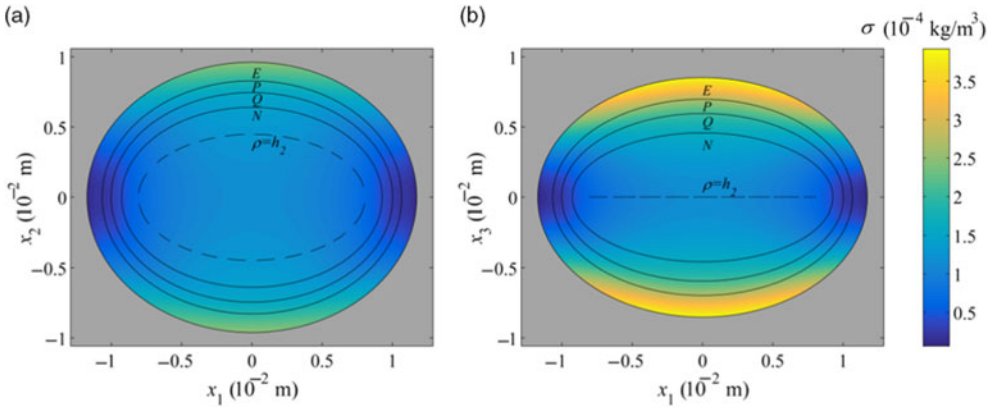

FIGURE 2. Nutrient concentration at constant pressure application $p^1_{\infty,0}(\rho_E)=15\times10^{-4}\,\text{kg/ms}^2$ for different intersections with the (a) x_1x_2-plane and (b) x_1x_3-plane.

Considering the values for l up to $l_{\max}\equiv M=4$ $(m=1,2,\ldots,2l+1)$, we plot the nutrient concentration and the pressure field from expansions (3.12) and (3.14), respectively. The numerical implementation is obtained for two different intersections of the tumour's structure with the coordinate planes, i.e. with the x_1x_2 -plane (see Figures 2(a) and 3(a)) and the x_1x_3-plane (see Figures 2(b) and 3(b)).

We observe that in Figure 2 the nutrient concentration values are higher in regions of low curvature and lower in regions of high curvature, as in the vicinity of the x_1-axis. On the other hand, the pressure field in Figure 3 is increasing as we move outwards from the necrotic region to the external surface S_E, which is an expected result, since we imply a uniform constant high pressure field on $\rho=\rho_E$ and sink terms in the corresponding partial differential equations. The obvious discontinuity 'ring' at the domain Ω_E is due to the Young–Laplace condition (2.20). A discussion on these findings is attempted below, together with the results of the following case.

https://doi.org/10.1017/S0956792518000499 Published online by Cambridge University Press

Table 2. *The coefficients of the pressure's exterior application* $p^m_{\infty,l}(\rho_E)$ *up to* $l=4$ $(m=1,2,\ldots,2l+1)$ $\left(10^{-4}\mathrm{kg/m^{2l+1}s^2}\right)$

	l				
m	0	1	2	3	4
1	$1.50000\times10^{+01}$	6.95991×10^{-13}	$6.77623\times10^{+00}$	-7.50844×10^{-12}	$2.64611\times10^{+01}$
2		-7.90147×10^{-20}	$-1.01606\times10^{+01}$	3.43444×10^{-12}	$-5.85472\times10^{+01}$
3		-2.93012×10^{-18}	-3.07941×10^{-19}	-3.46695×10^{-20}	$3.70038\times10^{+01}$
4			-2.41002×10^{-19}	-1.23844×10^{-20}	-2.11371×10^{-19}
5			9.57613×10^{-20}	7.93579×10^{-20}	3.06794×10^{-19}
6				-1.42574×10^{-20}	7.66247×10^{-20}
7				-2.27122×10^{-19}	8.43165×10^{-19}
8					-3.83254×10^{-20}
9					4.55415×10^{-22}

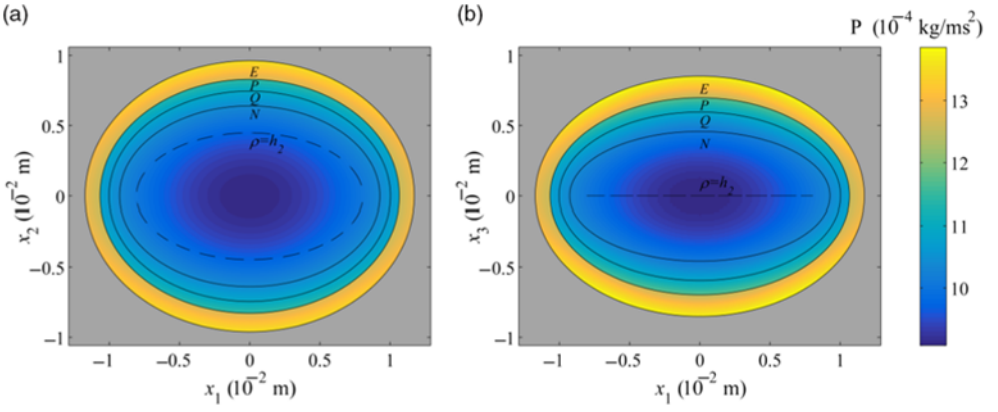

FIGURE 3. Pressure distribution at constant pressure application $p^1_{\infty,0}(\rho_E)=15\times10^{-4}\mathrm{kg/ms^2}$ for different intersections with the (a) x_1x_2-plane and (b) x_1x_3-plane.

In the next case we consider constant nutrient supply $\sigma^1_{\infty,0}(\rho_E)=2.5\times10^{-4}\,\mathrm{kg/m^3}$ on S_E, whereas $\sigma^m_{\infty,l}(\rho_E)=0$ for $l\geq1$ and $m=1,2,\ldots,2l+1$. Again, from (3.21) and (3.22), we evaluate the coefficients of the pressure's field on $\rho=\rho_E$ from (2.6), those being $p^m_{\infty,l}(\rho_E)$ for $l\geq0$ (up to $l=10$) and $m=1,2,\ldots,2l+1$, setting $p^1_{\infty,0}(\rho_E)=15\times10^{-4}\,\mathrm{kg/ms^2}$, convergence being attained at $l=l_{\max}\equiv M=4$ for the pressure's field and at $l=l_{\max}\equiv M=2$ for the nutrient's and inhibitor's field. In Table 2, we present the corresponding pressure's coefficients $p^m_{\infty,l}(\rho_E)$ up to the maximum value of $l=4$ $(m=1,2,\ldots,2l+1)$.

Plotting the nutrient and the pressure from series expansions (3.12) and (3.14) up to $l=l_{\max}\equiv M=4$ and $l=l_{\max}\equiv M=2$, respectively $(m=1,2,\ldots,2l+1)$, we take the two tumour's intersections, i.e. with the x_1x_2-plane (see Figures 4(a) and 5(a)) and the x_1x_3-plane (see Figures 4(b) and 5(b)).

Comparing the behaviour of the nutrient concentration depicted in Figure 4 and the pressure field as shown in Figure 5 with the corresponding situation described earlier for a constant pressure imposition, we observe that for the present case of a constant nutrient supply on the exterior

https://doi.org/10.1017/S0956792518000499 Published online by Cambridge University Press

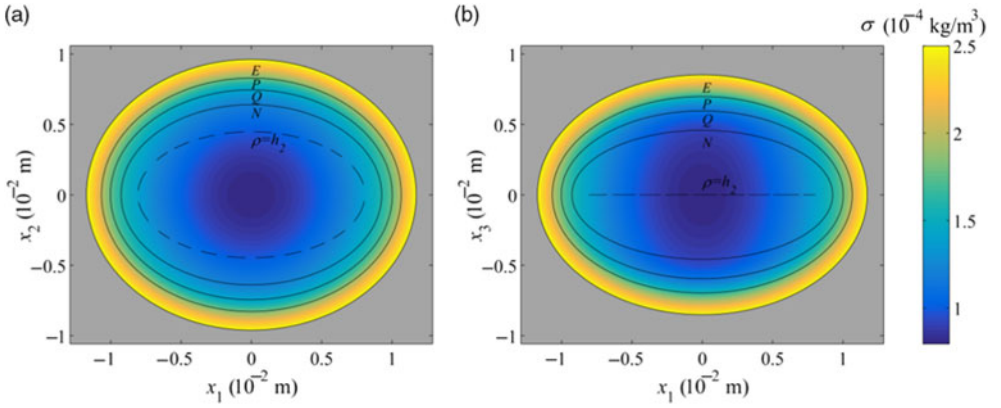

FIGURE 4. Nutrient concentration at a constant nutrient supply $\sigma^1_{\infty,0}(\rho_E) = 2.5 \times 10^{-4}$ kg/m^3 for different intersections with the (a) x_1x_2-plane and (b) x_1x_3-plane.

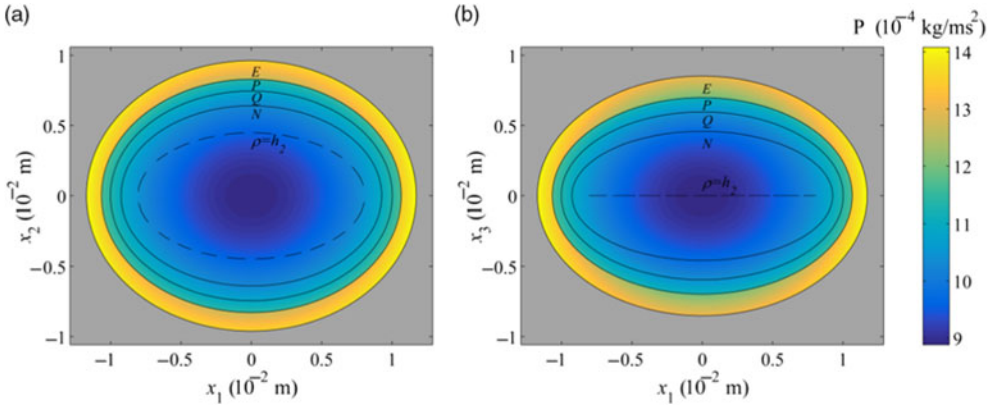

FIGURE 5. Pressure distribution at a constant nutrient supply $\sigma^1_{\infty,0}(\rho_E) = 2.5 \times 10^{-4}$ kg/m^3 for different intersections with the (a) x_1x_2-plane and (b) x_1x_3-plane.

tumour's compartment the relative distribution occurs in a quite different way. In fact, the nutrient concentration field is positive and increasing in the outward direction, while the pressure field is also an increasing function, which is larger on the tips of the x_1-axis, where the mean curvature is higher.

As a short comment to these findings, we note that the observed distributions are due to corresponding imposed nutrient and pressure field data. For example, in the first set of numerical experiments, we see that the imposed nutrient supply exhibits higher concentration in regions with less curvature and vice versa. The continuity of the normal flow of nutrient produces the rather surprising concentration profile especially along the x_1-axis. For example, regions of very low nutrient concentration occur in living layers along the x_1-axis, or regions of high nutrient along x_3-axis, easily explained as reflections of the corresponding profile of the nutrient field supplied externally. Nevertheless, biologically speaking, this is not so easily explained in accordance to the model assumptions since, the low concentration values in regions along x_1-axis do

https://doi.org/10.1017/S0956792518000499 Published online by Cambridge University Press

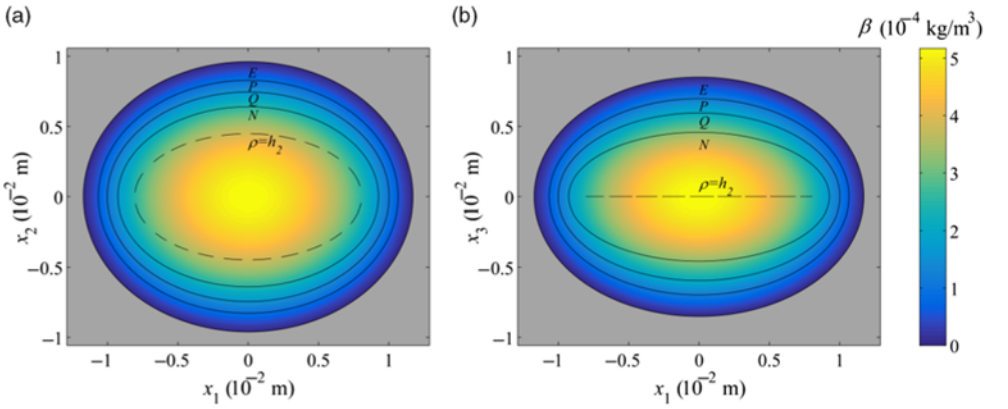

FIGURE 6. Inhibitor concentration either at a constant pressure application $p^1_{\infty,0}(\rho_E) = 15 \times 10^{-4}\,\mathrm{kg/ms^2}$ or with a constant nutrient supply $\sigma^1_{\infty,0}(\rho_E) = 2.5 \times 10^{-4}\,\mathrm{kg/m^3}$ for different intersections with the (a) x_1x_2-plane and (b) x_1x_3-plane.

not support cell survival, yet referring to living layers while, along x_3-axis, one could observe regions with nutrient values high enough to sustain cell life even if included in the necrotic core.

Having no available biological reference to support such findings in our knowledge, we suggest two scenarios to explain them, in biological terms. The first one suggests that we are confronted with a model artefact which indicates that the imposed data do not produce a physically acceptable solution. In this case, the fragility of the existence of the model's solution according to the model parameters is pointed out as well as the need for further investigation on the conditions that secure a physically concise solution to the model under consideration. A second scenario suggests that the model's layered structure should be considered as a geometrical configuration, corresponding to a more blurred material one, where the material layers are separated with layer boundaries rather than by strict boundary surfaces. In the transition zones, cells can be in either state, with respect to the nutrient or the inhibitor.

Referring to the pressure field's outwardly increasing profile, a supporting biological argument would suggest that, under the certain parameter values used for the numerical experiments presented ($F_N = 20\,\mathrm{kg/m^3s^2}$, $F_Q = 30\,\mathrm{kg/m^3s^2}$ and $F_P = 40\,\mathrm{kg/m^3s^2}$), the net cell gain ratio in each region together with the externally supplied pressure values provides pressure gradient directed towards the more active proliferating cells and the corresponding more populated layer.

Independently of the imposed exterior conditions of either constant pressure application or constant nutrient supply, the inhibitor concentration (3.13) remains unaffected for both cases, as it is readily expected. Hence, since this field is finite, needing only $l = 0, 1, 2$ and $m = 1, 2, \ldots, 2l + 1$, accuracy is then achieved immediately and the numerical plotting of β is depicted in Figure 6.

The inhibitor concentration field (3.13) admits a uniform behaviour shown in Figure 6, where obviously this field, on the contrary to the nutrient, decreases as we move outwards to the tumour's structure.

Our final task is to numerically solve the evolution equation in order to predict the evolution of the tumour's exterior boundary $\rho_P = \rho_P(t)$, which comprises relationship (3.19). In order to accomplish that, we have to take into consideration that the boundaries ρ_N, ρ_Q, ρ_P and ρ_E are now time-dependent, a fact that did not enter the previous calculations, since the corresponding

https://doi.org/10.1017/S0956792518000499 Published online by Cambridge University Press

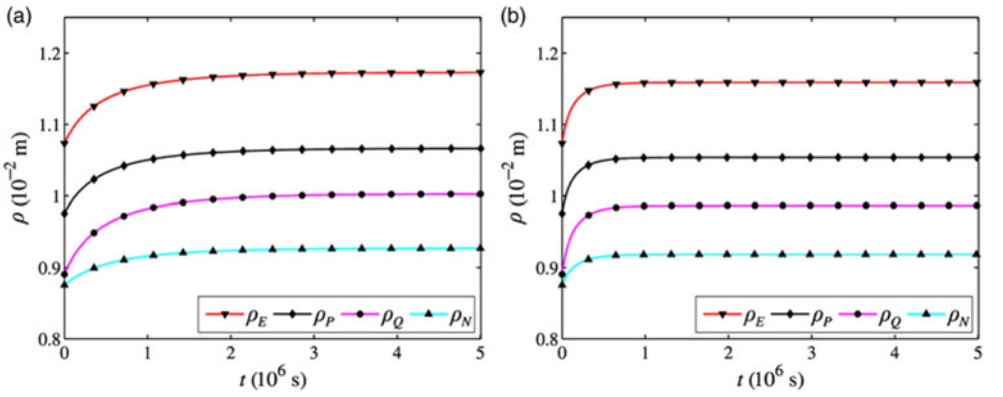

FIGURE 7. Time dependence of ρ_N, ρ_Q, ρ_P and ρ_E for different values of the proportionality constants (a) $(\mu_\sigma, \mu_\beta, \mu_P) = (6.77\,\mathrm{m}^5/\mathrm{kgs}, 8.04\,\mathrm{m}^5/\mathrm{kgs}, 13.3\,\mathrm{m}^3\mathrm{s}/\mathrm{kg}) \times 10^{-7}$ and (b) $(\mu_\sigma, \mu_\beta, \mu_P) = (2.25\,\mathrm{m}^5/\mathrm{kgs}, 2.77\,\mathrm{m}^5/\mathrm{kgs}, 4.54\,\mathrm{m}^3\mathrm{s}/\mathrm{kg}) \times 10^{-6}$.

boundary value problems described static processes. But they are also dependent among each other via (3.15)–(3.17). Hence, now, we work as follows. We assume the known values of $\sigma_N^* = 1.25 \times 10^{-4}\,\mathrm{kg/m^3}$, $\sigma_Q^* = 1.4 \times 10^{-4}\,\mathrm{kg/m^3}$ and $\beta^* = 1.6 \times 10^{-4}\,\mathrm{kg/m^3}$, while we solve numerically the nonlinear system of (3.15)–(3.17) for $\sigma_{\infty,0}^1(\rho_E) = 2.5 \times 10^{-4}\,\mathrm{kg/m^3}$, in order to define ρ_N, ρ_Q and ρ_E as a function of ρ_P. Then, we substitute these into the evolution equation (3.19), where one has to solve a nonlinear ordinary differential equation with respect to $\rho_P = \rho_P(t)$ with an initial condition $\rho_P(0) = 0.97 \times 10^{-2}\,\mathrm{m}$. The curves for the set $(\mu_\sigma, \mu_\beta, \mu_P) = (6.77\,\mathrm{m}^5/\mathrm{kgs}, 8.04\,\mathrm{m}^5/\mathrm{kgs}, 13.3\,\mathrm{m}^3\mathrm{s}/\mathrm{kg}) \times 10^{-7}$, used in all the previous calculations, are drawn in Figure 7(a). In order to further validate our modelling method, we proceeded to the implementation of all fields for slightly different (equilibrium state) boundaries $\rho_N = 0.918 \times 10^{-2}\,\mathrm{m}$, $\rho_Q = 1.053 \times 10^{-2}\,\mathrm{m}$, $\rho_P = 1.053 \times 10^{-2}\,\mathrm{m}$ and $\rho_E = 1.159 \times 10^{-2}\,\mathrm{m}$, as well for a different set of the aforementioned constants $(\mu_\sigma, \mu_\beta, \mu_P) = (2.25\,\mathrm{m}^5/\mathrm{kgs}, 2.77\,\mathrm{m}^5/\mathrm{kgs}, 4.54\,\mathrm{m}^3\mathrm{s}/\mathrm{kg}) \times 10^{-6}$, keeping all the other parameters the same. For reasons of clarity, we omit the presentation of the nutrient's and the inhibitor's concentrations, as well as the pressure field, since they behave similarly to those as demonstrated in Figures 2–6. However, we provide within Figure 7(b) the time-evolution of the corresponding tumour's boundaries.

The results demonstrate the evolution of the tumour's boundaries with respect to time and show excellent accordance with theory, since as the time increases, the boundaries ρ_N, ρ_Q, ρ_P and ρ_E reach limiting constant values, which coincide with those of the equilibrium stage, validating our approach.

6 Conclusions

In the present work, we presented a continuous non-symmetrical model of avascular tumour growth that evolves maintaining an ellipsoidal multilayer structure, lying inside a finite confocal ellipsoidal host layer and enjoying piecewise constant physical parameters, as tissue densities, diffusion constants, chemical consumption or production rates, cell motility parameters, cell proliferation or cell loss rate. This model belongs to a series of analytical works [9, 18, 22–24] on studying analytically the effect of geometric symmetry on modelling avascular growth,

https://doi.org/10.1017/S0956792518000499 Published online by Cambridge University Press

adopting the above simplifications in order to make the geometric effect clearer. Dropping such simplifications in favour of more realistic modelling is part of our future investigation.

These studies share the following features. First, inhomogeneous nutrient and pressure data, imposed by the tumour's microenvironment, are taken under consideration. Moreover, the degrees of freedom implied by non-symmetric geometries allow for improving the geometrical modelling by better fitting to a solid tumour. Especially, the ellipsoidal geometry offers the best fitting by allowing an appropriate adjustment of the two eccentricities of the ellipsoid and of its orientation to the tumour structure at hand. These two features, assigned to the ellipsoidal model presented in this work, make it the most general analytic model in studying the avascular tumours under a certain class of assumptions. Second, a homogeneous layer of healthy tissue, affected by the cancerous growth and lying in its immediate vicinity, is considered to follow the growth, being stiffer and denser than the rest of the host environment. Consequently, this healthy compartment is incorporated in the tumour's structure, its growth is also studied and moreover the model does not fail to consider it as a fluid of different phase than both the cancer tumour and the host surrounding medium. Finally, the cell movement is considered both as passively driven from the pressure gradients and as an active chemotactic response to the chemicals present to the cell's microenvironment, namely the nutrient and the inhibitor.

These features are all reflected in the results obtained for the nutrient field, the internally produced inhibitor field and the pressure field throughout the ellipsoidal tumour, as well as in the host layer in terms of ellipsoidal expansions. Connection formulae between all the tumour's interfaces are provided by means of the model's critical concentration values. The model predicts the evolution of the tumour's compartments in terms of a nonlinear ordinary differential equation with respect to the tumour's exterior boundary. The evolution equation is studied numerically and the corresponding numerical results are also included, for two special cases that the imposed pressure field and/or the nutrient field attribute ellipsoidal characteristics. It turns out that the deviation from the spherical symmetry and from the surrounding medium's homogeneity, as depicted in the aforementioned previous works and confirmed in this context, exhibits the following three characteristics.

First, the geometrical interfaces that distinguish the different tumour compartments cannot be defined by constant concentration values of the nutrient and of the inhibitor, as dictated by the physical model. Therefore, they have to be considered as ideal surfaces that do not coincide with the material interfaces, which are defined as the locus of the points that attribute the constant critical concentration values.

In the sequel, a special condition should hold between the nutrient data and the pressure data imposed by the tumour's surrounding medium, in order for the non-symmetrical growth to be realisable in a configuration that may depart significantly from being spherical. This feature is also present in more symmetrical models describing spheroidal or spherical tumour growth. In particular, the less symmetrical is the geometrical model, the more intricate this condition becomes. Nevertheless, this condition is not present when small perturbations from the spherical structure is considered, restricting asymmetrical growth to a slight deviation from the radial development, as shown in several works by stability analysis – see e.g. [6] and [28].

The third characteristic is that the non-symmetrical models offer the rather realistic feature that the tumour colony springs out from a group of cells, occupying a dimensional region, rather than a single cell, as demanded in the case of the spherically symmetric modelling. From the geometrical point of view, this is due to the fact that the ellipsoidal system springs out from the

2D focal ellipse, as well as the oblate spheroidal system, that springs out from the focal circle, modelling a mutated cell membrane that can start the building of a cancerous colony. Similarly, the prolate spheroidal model inherits the model a cell fibre initiating the tumour, by means of the focal segment of the system, while a spherical tumour can only be arisen from a single cell located at the centre of the colony. From a biological point of view, such characteristic may reflect both the hypothesis of polyclonic origin of some preneoplastic lesions, which involve several mutations in many cells before a cancer tumour occurs [34], and the spread of the mutated clone of a single cell as it evolves and establishes itself in the host tissue, appealing to the hypothesis of monoclonic origin of tumours [14]. In any case, using a manifold in $\mathbb{R}^n$ with $n \geq 1$, for modelling the spatial origin of tumour development, rather than a non-dimensional central point offers, to our opinion, a modelling advantage for incorporating the hypothesis of either a monoclonic, polyclonic or patch spread scenario for the origin of the tumour colony.

Conflict of interest

None.

Appendix A

In the interest of making this work complete and independent, we provide here some basic steps concerning specific analytical manipulations to obtain the particular solutions, given by expression (3.5) with (3.6) and the main implicated fields, provided via the compact series forms (3.12)–(3.14) with (3.7)–(3.11).

A1 Poisson's equation particular solution

Each Poisson's partial differential equation (2.8), (2.9) and (2.16), has a constant non-homogeneous term, whereas since the Laplace's operator possesses partial derivatives up to the second order, the general form of the most simple particular solution that should be used is a quadratic-form polynomial up to order two in terms of the three Cartesian coordinates x_1, x_2 and x_3, i.e.

$$f_{part,j}(\mathbf{r}) = a_{11}x_1^2 + a_{22}x_2^2 + a_{33}x_3^2 + 2a_{12}x_1x_2 + 2a_{13}x_1x_3 + 2a_{23}x_2x_3 + b_1x_1 + b_2x_2 + b_3x_3, \tag{A1}$$

where a_{11}, a_{22}, a_{33}, a_{12}, a_{13}, a_{23}, b_1, b_2 and b_3 are arbitrary constants to be calculated accordingly. The ellipsoidal representation of the Cartesian variables within (A1) is the key in finding the appropriate particular solution. In details, the Lamé functions of degree two [8] are given by

$$E_2^1(x) = x^2 + \Lambda - a_1^2, \tag{A2}$$

$$E_2^2(x) = x^2 + \Lambda' - a_1^2, \tag{A3}$$

$$E_2^3(x) = x\sqrt{|x^2 - h_3^2|}, \tag{A4}$$

$$E_2^4(x) = x\sqrt{|x^2 - h_2^2|} \tag{A5}$$

https://doi.org/10.1017/S0956792518000499 Published online by Cambridge University Press

and

$$E_2^5(x) = \sqrt{|x^2 - h_3^2|}\sqrt{|x^2 - h_2^2|}, \tag{A6}$$

where Λ and Λ' are the roots of the equation

$$\sum_{i=1}^{3} \frac{1}{\Lambda - \alpha_i^2} = 0, \tag{A7}$$

from which we obtain

$$(x - \Lambda)\left(x - \Lambda'\right) = x^2 - \frac{2\left(\alpha_1^2 + \alpha_2^2 + \alpha_3^2\right)}{3}x + \frac{\alpha_1^2\alpha_2^2 + \alpha_2^2\alpha_3^2 + \alpha_3^2\alpha_1^2}{3} = 0. \tag{A8}$$

Bearing in mind (A2) and (A3), the corresponding surface ellipsoidal harmonics read as

$$S_2^1(\mu, \nu) := E_2^1(\mu)\, E_2^1(\nu) = \mu^2\nu^2 + \left(\Lambda - \alpha_1^2\right)\left(\mu^2 + \nu^2\right) + \left(\Lambda - \alpha_1^2\right)^2 \tag{A9}$$

and

$$S_2^2(\mu, \nu) := E_2^2(\mu)\, E_2^2(\nu) = \mu^2\nu^2 + \left(\Lambda' - \alpha_1^2\right)\left(\mu^2 + \nu^2\right) + \left(\Lambda' - \alpha_1^2\right)^2, \tag{A10}$$

which leads to the expression

$$\mu^2\nu^2 = \left(\Lambda - \alpha_1^2\right)\left(\Lambda' - \alpha_1^2\right)\left[1 - \frac{S_2^1(\mu, \nu)}{\left(\Lambda - \Lambda'\right)\left(\Lambda - \alpha_1^2\right)} + \frac{S_2^2(\mu, \nu)}{\left(\Lambda - \Lambda'\right)\left(\Lambda' - \alpha_1^2\right)}\right]. \tag{A11}$$

But, from (A8), via the substitution $x = \alpha_1^2$, it follows that

$$\left(\alpha_1^2 - \Lambda\right)\left(\alpha_1^2 - \Lambda'\right) = \frac{1}{3}\left(\alpha_1^2 - \alpha_3^2\right)\left(\alpha_1^2 - \alpha_2^2\right) = \frac{1}{3}h_2^2h_3^2, \tag{A12}$$

hence, taking into account that $S_0^1(\mu, \nu) = 1$, relation (A11) is written as

$$\mu^2\nu^2 = \frac{1}{3}h_2^2h_3^2\left[S_0^1(\mu, \nu) - \frac{S_2^1(\mu, \nu)}{\left(\Lambda - \Lambda'\right)\left(\Lambda - \alpha_1^2\right)} + \frac{S_2^2(\mu, \nu)}{\left(\Lambda - \Lambda'\right)\left(\Lambda' - \alpha_1^2\right)}\right], \tag{A13}$$

which, by substitution in (2.2), gives

$$x_1^2 = \frac{\rho^2}{3}\left[S_0^1(\mu, \nu) - \frac{S_2^1(\mu, \nu)}{\left(\Lambda - \Lambda'\right)\left(\Lambda - \alpha_1^2\right)} + \frac{S_2^2(\mu, \nu)}{\left(\Lambda - \Lambda'\right)\left(\Lambda' - \alpha_1^2\right)}\right]. \tag{A14}$$

Similarly, it can be shown that

$$x_2^2 = \frac{\rho^2 - h_3^2}{3}\left[S_0^1(\mu, \nu) - \frac{S_2^1(\mu, \nu)}{\left(\Lambda - \Lambda'\right)\left(\Lambda - \alpha_2^2\right)} + \frac{S_2^2(\mu, \nu)}{\left(\Lambda - \Lambda'\right)\left(\Lambda' - \alpha_2^2\right)}\right] \tag{A15}$$

and

$$x_3^2 = \frac{\rho^2 - h_2^2}{3}\left[S_0^1(\mu, \nu) - \frac{S_2^1(\mu, \nu)}{\left(\Lambda - \Lambda'\right)\left(\Lambda - \alpha_3^2\right)} + \frac{S_2^2(\mu, \nu)}{\left(\Lambda - \Lambda'\right)\left(\Lambda' - \alpha_3^2\right)}\right]. \tag{A16}$$

https://doi.org/10.1017/S0956792518000499 Published online by Cambridge University Press

Next, from (A4)–(A6) with respect to (2.2)–(2.4) and straightforward calculations, it is valid that

$$x_1 x_2 = \frac{\rho\sqrt{|\rho^2 - h_3^2|}}{h_1 h_2 h_3^2} S_2^3(\mu, \nu), \tag{A17}$$

$$x_1 x_3 = \frac{\rho\sqrt{|\rho^2 - h_2^2|}}{h_1 h_2^2 h_3} S_2^4(\mu, \nu) \tag{A18}$$

and

$$x_2 x_3 = \frac{\sqrt{|\rho^2 - h_3^2|}\sqrt{|\rho^2 - h_2^2|}}{h_1^2 h_2 h_3} S_2^5(\mu, \nu). \tag{A19}$$

On the other hand, using the Lamé functions of the first degree [8]

$$E_1^1(x) = x, \tag{A20}$$

$$E_1^2(x) = \sqrt{|x^2 - h_3^2|} \tag{A21}$$

and

$$E_1^3(x) = \sqrt{|x^2 - h_2^2|}, \tag{A22}$$

then, from (2.2)–(2.4), we readily obtain

$$x_1 = \frac{\rho}{h_2 h_3} S_1^1(\mu, \nu), \tag{A23}$$

$$x_2 = \frac{\sqrt{|\rho^2 - h_3^2|}}{h_1 h_3} S_1^2(\mu, \nu) \tag{A24}$$

and

$$x_3 = \frac{\sqrt{|\rho^2 - h_2^2|}}{h_1 h_2} S_1^3(\mu, \nu). \tag{A25}$$

Consequently, with respect to (A14)–(A16), (A17)–(A19) and (A23)–(A25), the Cartesian representation (A1) admits an equivalent ellipsoidal form. However, all the terms are not needed, since if we demand (A1) to satisfy each similar Poisson's equations (2.8), (2.9) and (2.16), we implement trivial calculations, showing that $a_{11} + a_{22} + a_{33} = A_j/2$, in terms of $A_j \equiv \gamma_j, p_j, F_j$, respectively for $j = N, Q, P, E$, while $a_{12}, a_{13}, a_{23}, b_1, b_2$ and b_3 can take any value in $\mathbb{R}$. Though we search for one particular solution, we may set $a_{22} = a_{33} = a_{12} = a_{13} = a_{23} = b_1 = b_2 = b_3 = 0$ and $a_{11} = A_j/2$, as it is obvious to look for a simple expression. Henceforth, gathering the above information for the arbitrary constants in (A1), it becomes

$$f_{part,j}(\mathbf{r}) = \frac{A_j \rho^2}{6}\left[E_0^1(\mu)\, E_0^1(\nu) - \frac{E_2^1(\mu)\, E_2^1(\nu)}{(\Lambda - \Lambda')(\Lambda - \alpha_1^2)} + \frac{E_2^2(\mu)\, E_2^2(\nu)}{(\Lambda - \Lambda')(\Lambda - \alpha_1^2)}\right] \text{for } j = N, Q, P, E, \tag{A26}$$

which is actually the expressions (3.5) with (3.6), expressed in terms of surface ellipsoidal harmonics.

https://doi.org/10.1017/S0956792518000499 Published online by Cambridge University Press

A2 Model's boundary value problems

Under the aim to show the main analytical steps in order to reach the final expressions for the nutrient concentration (3.12), the inhibitor concentration (3.13) and the pressure field (3.14), we are initially dealt with the determination of the nutrient concentration field. It is assumed to satisfy the boundary value problem

$$\Delta\sigma_j(\mathbf{r}) = \gamma_j \text{ for } \mathbf{r} \in \Omega_j \text{ with } j = N, Q, P, \tag{A27}$$

while

$$\Delta\sigma_E(\mathbf{r}) = 0 \text{ for } \mathbf{r} \in \Omega_E, \tag{A28}$$

with boundary conditions

$$\sigma_Q(\mathbf{r}) = \sigma_N\,(\mathbf{r}) \;\text{ for } \mathbf{r} \in S_N, \tag{A29}$$

$$\frac{\partial}{\partial\rho}\sigma_Q(\mathbf{r}) - \frac{\partial}{\partial\rho}\sigma_N\,(\mathbf{r}) = 0, \;\text{ for } \mathbf{r} \in S_N, \tag{A30}$$

as well as

$$\sigma_P(\mathbf{r}) = \sigma_Q(\mathbf{r}) \text{ for } \mathbf{r} \in S_Q, \tag{A31}$$

$$\frac{\partial}{\partial\rho}\sigma_P(\mathbf{r}) - \frac{\partial}{\partial\rho}\sigma_Q(\mathbf{r}) = 0 \text{ for } \mathbf{r} \in S_Q \tag{A32}$$

and

$$\sigma_E(\mathbf{r}) = \sigma_P(\mathbf{r}) \text{ for } \mathbf{r} \in S_P, \tag{A33}$$

$$\frac{\partial}{\partial\rho}\sigma_E(\mathbf{r}) - \frac{\partial}{\partial\rho}\sigma_P(\mathbf{r}) = 0 \text{ for } \mathbf{r} \in S_P, \tag{A34}$$

whereas on the exterior boundary S_E, we have the expansion

$$\sigma_E = \sigma_\infty(\mathbf{r}_E) = \sigma_\infty(\rho_E, \mu, \nu) = \sum_{l=0}^{\infty}\sum_{m=1}^{2l+1} \sigma_{\infty,l}^m(\rho_E)\, S_l^m(\mu, \nu), \tag{A35}$$

as (2.5) dictates, where in view of the orthogonality relationship (3.4), it holds

$$\sigma_{\infty,l}^m(\rho_E) = \frac{1}{\gamma_l^m} \iint\limits_{S_{\rho_E}} S_l^m(\mu, \nu)\, \sigma_\infty(\rho_E, \mu, \nu) \frac{ds(\mu, \nu)}{\sqrt{\rho_j^2 - \mu^2}\sqrt{\rho_j^2 - \nu^2}}. \tag{A36}$$

The expansions of the nutrient concentration in each domain are written as

$$\sigma_N(\mathbf{r}) = f_{part,N}(\rho, \mu, \nu) + \sum_{l=0}^{\infty}\sum_{m=1}^{2l+1} a_{\sigma,l}^{(i)m} E_l^m(\rho)\, S_l^m(\mu, \nu) \text{ for } \mathbf{r} \in \Omega_N, \tag{A37}$$

$$\sigma_Q(\mathbf{r}) = f_{part,Q}(\rho, \mu, \nu) + \sum_{l=0}^{\infty}\sum_{m=1}^{2l+1} \left[b_{\sigma,l}^{(i)m} + b_{\sigma,l}^{(e)m}(2n+1)\, I_l^m(\rho) \right] E_l^m(\rho)\, S_l^m(\mu, \nu) \text{ for } \mathbf{r} \in \Omega_Q, \tag{A38}$$

https://doi.org/10.1017/S0956792518000499 Published online by Cambridge University Press

$$\sigma_P(\mathbf{r}) = f_{part,P}(\rho,\mu,\nu) + \sum_{l=0}^{\infty}\sum_{m=1}^{2l+1}\left[c_{\sigma,l}^{(i)m} + c_{\sigma,l}^{(e)m}(2n+1)\,I_l^m(\rho)\right]E_l^m(\rho)\,S_l^m(\mu,\nu) \text{ for } \mathbf{r}\in\Omega_P \tag{A39}$$

and

$$\sigma_E(\mathbf{r}) = \sum_{l=0}^{\infty}\sum_{m=1}^{2l+1}\left[d_{\sigma,l}^{(i)m} + d_{\sigma,l}^{(e)m}(2n+1)\,I_l^m(\rho)\right]E_l^m(\rho)\,S_l^m(\mu,\nu) \text{ for } \mathbf{r}\in\Omega_E, \tag{A40}$$

where $f_{part,j}(\rho,\mu,\nu)$ is given by (3.5), substituting $A_j=\gamma_j$ for $j=N,Q,P$. Applying boundary conditions (A29)–(A35) into expansions (A37)–(A40) with (A36) and using the orthogonality relation (3.4) and the notation (3.6), we obtain, respectively, for $l\geq 0$ and $m=1,2,...,2l+1$

$$E_l^m(\rho_N)\left(a_{\sigma,l}^{(i)m} - b_{\sigma,l}^{(i)m}\right) - F_l^m(\rho_N)\,b_{\sigma,l}^{(e)m} = \left(\gamma_Q-\gamma_N\right)\rho_N^2 d_l^m, \tag{A41}$$

$$E_l^{m'}(\rho_N)\left(a_{\sigma,l}^{(i)m} - b_{\sigma,l}^{(i)m}\right) - F_l^{m'}(\rho_N)\,b_{\sigma,l}^{(e)m} = 2(\gamma_Q-\gamma_N)\,\rho_N d_l^m, \tag{A42}$$

$$E_l^m(\rho_Q)\left(b_{\sigma,l}^{(i)m} - c_{\sigma,l}^{(i)m}\right) + F_l^m(\rho_Q)\left(b_{\sigma,l}^{(e)m} - c_{\sigma,l}^{(e)m}\right) = \left(\gamma_P-\gamma_Q\right)\rho_Q^2 d_l^m, \tag{A43}$$

$$E_l^{m'}(\rho_Q)\left(b_{\sigma,l}^{(i)m} - c_{\sigma,l}^{(i)m}\right) + F_l^{m'}(\rho_Q)\left(b_{\sigma,l}^{(e)m} - c_{\sigma,l}^{(e)m}\right) = 2(\gamma_P-\gamma_Q)\,\rho_Q d_l^m, \tag{A44}$$

$$E_l^m(\rho_P)\left(c_{\sigma,l}^{(i)m} - d_{\sigma,l}^{(i)m}\right) + F_l^m(\rho_P)\left(c_{\sigma,l}^{(e)m} - d_{\sigma,l}^{(e)m}\right) = -\gamma_P\rho_P^2 d_l^m, \tag{A45}$$

$$E_l^{m'}(\rho_P)\left(c_{\sigma,l}^{(i)m} - d_{\sigma,l}^{(i)m}\right) + F_l^{m'}(\rho_P)\left(c_{\sigma,l}^{(e)m} - d_{\sigma,l}^{(e)m}\right) = -2\gamma_P\rho_P d_l^m \tag{A46}$$

and

$$E_l^m(\rho_E)\,d_{\sigma,l}^{(i)m} + F_l^m(\rho_E)\,d_{\sigma,l}^{(e)m} = \sigma_{\infty,l}^m(\rho_E). \tag{A47}$$

Solving the seventh-order linear system (A41)–(A47), with respect to the seven sequences of unknown coefficients, we arrive at the nutrient concentration field $\sigma_j\,(\rho,\mu,\nu)$ for each domain Ω_j with $j=N,Q,P,E$, which can be rewritten into a single expression using the Heaviside function (3.7) as

$$\begin{aligned}\sigma(\mathbf{r}) = {}& \sigma_N(\mathbf{r}) + H(\rho-\rho_N)\left(\sigma_Q\,(\mathbf{r}) - \sigma_N(\mathbf{r})\right)\\ & + H(\rho-\rho_Q)\left(\sigma_P(\mathbf{r}) - \sigma_Q(\mathbf{r})\right) + H(\rho-\rho_P)\left(\sigma_E(\mathbf{r}) - \sigma_P(\mathbf{r})\right),\end{aligned} \tag{A48}$$

which using the notation (3.8)–(3.11), yields the nutrient concentration field (3.12). Following exactly the same procedure as in the nutrient concentration, we obtain the inhibitor concentration field (3.13), which satisfies the boundary value problems (2.9), (2.11) and (2.14), where $\beta_E=0$ on S_E, using the non-trivial expansions

$$\beta_N(\mathbf{r}) = f_{part,N}\,(\rho,\mu,\nu) + \sum_{l=0}^{\infty}\sum_{m=1}^{2l+1} a_{\beta,l}^{(i)m}E_l^m(\rho)S_l^m(\mu,\nu) \text{ for } \mathbf{r}\in\Omega_N, \tag{A49}$$

$$\beta_Q(\mathbf{r}) = f_{part,Q}\,(\rho,\mu,\nu) + \sum_{l=0}^{\infty}\sum_{m=1}^{2l+1}\left[b_{\beta,l}^{(i)m} + b_{\beta,l}^{(e)m}(2n+1)I_l^m(\rho)\right]E_l^m(\rho)\,S_l^m(\mu,\nu) \text{ for } \mathbf{r}\in\Omega_Q, \tag{A50}$$

https://doi.org/10.1017/S0956792518000499 Published online by Cambridge University Press

$$\beta_P(\mathbf{r}) = f_{part,P}(\rho,\mu,\nu) + \sum_{l=0}^{\infty}\sum_{m=1}^{2l+1}\left[c_{\beta,l}^{(i)m} + c_{\beta,l}^{(e)m}(2n+1)\,I_l^m(\rho)\right]E_l^m(\rho)\,S_l^m(\mu,\nu) \text{ for } \mathbf{r}\in\Omega_P, \tag{A51}$$

and

$$\beta_E(\mathbf{r}) = \sum_{l=0}^{\infty}\sum_{m=1}^{2l+1}\left[d_{\beta,l}^{(i)m} + d_{\beta,l}^{(e)m}(2n+1)I_l^m\,(\rho)\right]E_l^m(\rho)\,S_l^m(\mu,\nu) \text{ for } \mathbf{r}\in\Omega_E, \tag{A52}$$

where $A_j = p_j$ for $j = N, Q, P$ and $p_Q = p_P := p_L$. In a very similar way, the boundary value problem for the pressure field (2.16)–(2.20) yields the solution (3.14), where the corresponding expansions read as

$$P_N(\mathbf{r}) = f_{part,N}(\rho,\mu,\nu) + \sum_{l=0}^{\infty}\sum_{m=1}^{2l+1} a_{P,l}^{(i)m}E_l^m(\rho)\,S_l^m(\mu,\nu) \text{ for } \mathbf{r}\in\Omega_N, \tag{A53}$$

$$P_Q(\mathbf{r}) = f_{part,Q}(\rho,\mu,\nu) + \sum_{l=0}^{\infty}\sum_{m=1}^{2l+1}\left[b_{P,l}^{(i)m} + b_{P,l}^{(e)m}(2n+1)\,I_l^m(\rho)\right]E_l^m(\rho)\,S_l^m(\mu,\nu) \text{ for } \mathbf{r}\in\Omega_Q, \tag{A54}$$

$$P_P(\mathbf{r}) = f_{part,P}\,(\rho,\mu,\nu) + \sum_{l=0}^{\infty}\sum_{m=1}^{2l+1}\left[c_{\mathrm{P},l}^{(i)m} + c_{\mathrm{P},l}^{(e)m}\,(2n+1)\,I_l^m\,(\rho)\right]E_l^m(\rho)\,S_l^m(\mu,\nu) \text{ for } \mathbf{r}\in\Omega_P, \tag{A55}$$

and

$$P_E(\mathbf{r}) = \sum_{l=0}^{\infty}\sum_{m=1}^{2l+1}\left[d_{P,l}^{(i)m} + d_{P,l}^{(e)m}\,(2n+1)\,I_l^m\,(\rho)\right]E_l^m(\rho)\,S_l^m(\mu,\nu) \text{ for } \mathbf{r}\in\Omega_E, \tag{A56}$$

where $A_j = F_j$ for $j = N, Q, P$, while the exterior pressure distribution $P_\infty(\mathbf{r}_E)$ on S_E is expanded as

$$P_\infty(\mathbf{r}_E) = \sum_{l=0}^{\infty}\sum_{m=1}^{2l+1} p_{\infty,l}^m(\rho_E)\,S_l^m(\mu,\nu),$$
$$\text{where } p_{\infty,l}^m(\rho_E) = \frac{1}{\gamma_l^m}\iint\limits_{S_{\rho_E}}\frac{S_l^m(\mu,\nu)\,P_\infty(\rho_E,\mu,\nu)\,ds(\mu,\nu)}{\sqrt{\rho_j^2-\mu^2}\sqrt{\rho_j^2-\nu^2}}. \tag{A57}$$

Obviously, the procedure for the calculation of the unknown constant coefficients within the inhibitor concentration (A49)–(A52) and the pressure field (A53)–(A56) leads to similar linear algebraic systems such as (A41)–(A47), the aforementioned fields are written in a concrete formalism similar to (A48) for the nutrient concentration field.

References

[1] Adam, J. A. (1987) A mathematical model of tumour growth. II. Effects of geometry and spatial nonuniformity on stability. *Math. Biosci.* **86**, 183–211. doi:10.1016/0025-5564(87)90010-1.

[2] Araujo, R. P. & McElwain, D. L. S. (2004) A history of the study of solid tumour growth: the contribution of mathematical modeling. *Bull. Math. Biol.* **66**, 1039–1091. doi:10.1016/j.bulm.2003.11.002.

https://doi.org/10.1017/S0956792518000499 Published online by Cambridge University Press

[3] BURTON, A. C. (1966) Rate of growth of solid tumors as a problem of diffusion. *Growth* **30**, 157–176.
[4] BYRNE, H. (1999) A weakly nonlinear analysis of a model of avascular solid tumour growth. *J. Math. Biol*. **39**, 59–89. doi:10.1007/s002850050163.
[5] BYRNE, H. M., ALARCON, T., OWEN, M. R., WEBB, S. D. & MAINI, P. K. (2006) Modelling aspects of cancer dynamics: a review. *Philos. Trans. R. Soc*. **364**, 1563–1578. doi:10.1098/rsta.2006.1786.
[6] BYRNE, H. M. & CHAPLAIN, M. A. J. (1996) Growth of necrotic tumors in the presence and absence of inhibitors. *Math. Biosci*. **135**, 187–216. doi:10.1016/0025-5564(96)00023-5.
[7] CHEN, C. Y., BYRNE, H. M. & KING, J. R. (2001) The influence of growth induced stress from the surrounding medium on the development of multicell spheroids. *J. Math. Biol*. **43**, 191–220. doi:10.1007/s002850100091.
[8] DASSIOS, G. (2012) *Ellipsoidal Harmonics. Theory and Applications*, Cambridge University Press, Cambridge.
[9] DASSIOS, G., KARIOTOU, F., SLEEMAN, B. D. & TSAMPAS, M. N. (2012) Mathematical modeling of the avascular ellipsoidal tumour growth. *Q. Appl. Math*. **70**, 1–24. doi:10.1090/S0033-569X-2011-01240-2.
[10] DASSIOS, G., KARIOTOU, F. & VAFEAS, P. (2013) Invariant vector harmonics. The ellipsoidal case. *J. Math. Anal. Appl*. **405**, 652–660. doi:10.1016/j.jmaa.2013.03.015.
[11] FASANO, A., BERTUZZI, A. & GANDOLFI, A. (2006) Mathematical modelling of tumour growth and treatment. In: A. QUARTERONI, L. FORMAGGIA, and A. VENEZIANI (editors), *Complex Systems in Biomedicine*, Springer–Verlag, Milano, pp. 71–108.
[12] FOLKMAN, J. & HOCHBERG, M. (1973) Self-regulation of growth in three dimensions. *J. Exp. Med*. **138**, 745–753. doi:10.1084/jem.138.4.745.
[13] FRIEDMAN, A. (2009) Free boundary problems associated with multiscale tumor models. *Math. Model. Nat. Pheno*. **4**, 134–155. doi:10.1051/mmnp/20094306.
[14] GARCIA, S. B., PARK, H. S., NOVELLI, M. & WRIGHT, N. A. (1999) Field cancerization, clonality and epithelial stem cells: the spread of mutated clones in epithelial sheets. *J. Pathol*. **187**, 61–81. doi:10.1002/(ISSN)1096-9896.
[15] GIVERSO, C. & CIARETTA, P. (2016) On the morphological stability of multicellular tumour spheroids growing in porous media. *Eur. Phys. J. E*. **39**(10), 92.
[16] GREENSPAN, H. P. (1972) Models for the growth of a solid tumor by diffusion. *Stud. Appl. Math*. **51**, 317–340. doi:10.1002/sapm.v51.4.
[17] GREENSPAN, H. P. (1976) On the growth and stability of cell cultures and solid tumors. *J. Theor. Biol*. **56**, 229–242. doi:10.1016/S0022-5193(76)80054-9.
[18] HADJINICOLAOU, M. & KARIOTOU, F. (2010) On the effect of 3D anisotropic tumour growth on modelling the nutrient distribution in the interior of the tumour. *Bull. Greek Math. Soc*. **57**, 189–197.
[19] HELMLINGER, G., NETTI, P. A., LICHTENBELD, H. D., MELDER, R. J. & JAIN, R. K. (1997) Solid stress inhibits the growth of multicellular tumour spheroids. *Nat. Biotechnol*. **15**, 778–783. doi:10.1038/nbt0897-778.
[20] HOBSON, E. W. (1965) *The Theory of Spherical and Ellipsoidal Harmonics*, Chelsea Publishing Company, New York.
[21] JONES, D. S. & SLEEMAN, B. D. (2008) Mathematical modeling of avascular and vascular tumor growth. *Adv. Topics Scatter. Biomed. Eng. World Sci*. 305–331. doi:10.1142/6865.
[22] KARIOTOU, F. & VAFEAS, P. (2012) The avascular tumour growth in the presence of inhomogeneous physical parameters imposed from a finite spherical nutritive environment. *Inter. J. Differ. Equ*. **2012**, 175434. doi:10.1186/1687-1847-2012-1.
[23] KARIOTOU, F. & VAFEAS, P. (2014) On the transversally isotropic pressure effect on avascular tumour growth. *Math. Methods Appl. Sci*. **37**, 277–282. doi:10.1002/mma.2789.
[24] KARIOTOU, F., VAFEAS, P. & PAPADOPOULOS, P. K. (2014) Mathematical modeling of tumour growth in inhomogeneous spheroidal environment. *Inter. J. Biol. Biomed. Eng*. **8**, 132–141.

[25] LOWENGRUB, J. S., FRIEBOES, H. B., JIN, F., CHUANG, Y.-L., LI, X., MACKLIN, P., WISE, S. M. & CHRISTINI, V. (2010) Nonlinear modelling of cancer: bridging the gap between cells and tumours. *Nonlinearity* **23**, R1–R9. doi:10.1088/0951-7715/23/1/R01.

[26] MOON, P. & SPENCER, D. E. (1988) *Field Theory Handbook*, Springer, Berlin.

[27] PLANK, M. J. & SLEEMAN, B. D. (2003) Tumour-induced angiogenesis: a review. *J. Theor. Med*. **5**, 137–153. doi:10.1080/10273360410001700843.

[28] PREZIOSI, L. (2003) *Cancer Modelling and Simulation*, Chapman & Hall/CRC, London.

[29] PREZIOSI, L. & TOSIN, A. (2009) Multiphase modelling of tumor growth and extra cellular matrix interaction: mathematical tools and applications. *J. Math. Biol*. **58**, 625–656. doi:10.1007/s00285-008-0218-7.

[30] ROOSE, T., CHAPMAN, S. J. & MAINI, P. K. (2007) Mathematical models of avascular tumor growth. *SIAM J. Appl. Math*. **49**, 179–208. doi:10.1137/S0036144504446291.

[31] SUTHERLAND, R. (1986) Importance of critical metabolites and cellular interactions in the biology of microregions of tumors. *Cancer* **58**, 1668–1680. doi:10.1002/(ISSN)1097-0142.

[32] SUTHERLAND, R. (1988) Cell and environment interactions in tumor microregions: the multicell spheroid model. *Science* **240**, 177–184. doi:10.1126/science.2451290.

[33] VOUTOURI, C., MPEKRIS, F., PAPAGEORGIS, P., ODYSSEOS, A. D., STYLIANOPOULOS, T. (2014) Role of constitutive behavior and tumor-host mechanical interactions in the state of stress and growth of solid tumors. *PLoS One* **9**(8), e104717. doi:10.1371/journal.pone.0104717.

[34] WRIGHT, N. A. (2002) Cell proliferation in carcinogenesis Chapter 18. In: M. R. ALISON (editor), *The Cancer Handbook*, Nature Publishing Group, MI, pp. 246–255.